

The Hebrew University of Jerusalem  
Faculty of Mathematics and Sciences  
Selim and Rachel Benin School of Engineering  
Applied Physics Department



# Polymeric waveguide platform fabrication optimization

אופטימיזציה בייצור פלטפורמה של מוליך גל  
עשוי מפולימרים

by

Moran Bin Nun

This work was done under the supervision of

Dr. Dan M. Marom

Thesis submitted for M.Sc. degree

January, 2013

## Acknowledgments

I first wish to thank my dear husband Gabriel for his endless support and encouragement through the research. I wish to thank him for staying with the children while I was working on this research. Without him, this work couldn't succeed.

I thank my advisor Dr. Dan Marom for his guidance and advices through the research. For his availability every time questions aroused. His guidance made me understand deeply every step I took in this research.

I wish to thank all the nanocenter staff at the Hebrew university: Dr Shimon Eliav, Mr. Rami Gabay , Mrs.Galina Chechelinsky, Mr. Mourice Saidian and Mr. Doron Greental for helping me both understand the process and acquire skills in the fabrication tools.

I wish to thank Dr. Shira Yochelis and Mrs. Inbal Davidi from the Chemistry department at the Hebrew university for helping me understand the chemistry behind my research.

Finally, I wish to thank God in heaven "because he gives us the strength to do this wealth".

# Abstract

In this work I report on the development of a platform of a polymeric waveguide composed of Cytop as the cladding and PFCB as the core. These two polymers were chosen due to their low loss in the optical communication regime (0.26 dB/cm for PFCB core and 0.022dB/cm for Cytop cladding). PFCB and Cytop have refractive indexes of 1.48 and 1.34 respectively and therefore offer high index contrast in comparison to glass waveguides. PFCB was chosen as the waveguide core since it has been proven a good host for nanocrystals (NCs).

In this work a lot of effort was invested in making the fabrication process compatible with semiconductor NCs that will in the long term be mixed in the PFCB core. Doping the core with nanocrystals is of interest, since the NCs properties are diverse, flexible and controllable. Choosing NCs with high third order susceptibility will allow us to fabricate nonlinear waveguides. Furthermore, specifying the NCs shape and size will allow us to align them by applying external electric voltage and by that enhance the macroscopic nonlinear properties of the composite.

Two fabrication configuration are proposed. Both are aimed at fabricating a square waveguide. The first configuration is the ridge-method where the PFCB core undergoes reactive ion etching (RIE). This method carries on with previously proposed methodology at the Photonic Devices Laboratory of Dr. Marom [1], however several key improvements were made.

The second configuration is the trench-method where only the Cytop undergoes RIE. By that method we wish to prevent roughness that might occur in the alternative method due to etching a composite made of PFCB and the NCs at the same time. In addition not all NC materials we would like to use are allowed into the RIE chamber since they may cause contamination to the RIE machine. Replacing the ridge method with the trench one will obviously overcome this obstacle. However both methods have their own challenges. In this work I tried to overcome some of the challenges and to produce reliable and reproducible method for fabricating a square polymeric waveguide compatible with NCs.

## תקציר

בעבודה זו אני מדווחת על ההתפתחות של פלטפורמה של מוליך גל פולימרי העשוי מ Cytop המשמש כמעטפת מוליך הגל ו PFCB המשמש כליבת מוליך הגל. שני פולימרים אלו נבחרו בשל ההפסדים הנמוכים שלהם בתחום התקשורת האופטית ( $0.022\text{dB/cm}$  עבור מעטפת ה Cytop ו  $0.026\text{dB/cm}$  עבור ליבת ה PFCB). גורמי השבירה של PFCB ו Cytop הם  $1.48$  ו  $1.34$  בהתאמה ולכן מציעים ניגודיות גבוהה בגורם השבירה בהשוואה למוליכי גלים העשויים מזכוכית. PFCB נבחר בתור הליבה של מוליך הגל מאחר והוכח כמארח טוב עבור ננו-חלקיקים.

בעבודה זו הושקע מאמץ רב על מנת שהתהליך יהיה תואם לדרישות של הננו-חלקיקים העתידים להיות בטווח הארוך מעורבבים בתוך ליבת ה PFCB. אילוח הליבה בננו-חלקיקים מוליכים למחצה (מל"מ) הינו דבר מעניין מאחר ותכונות הננו-חלקיקים הינן מגוונות, גמישות וניתנות לשליטה. בחירת ננו-חלקיקים בעלי סוספטביליות גבוהה מסדר שלישי תאפשר לנו לייצר מוליך גל לא לינארי. יתר על כן, תכנון הצורה והגודל של הננו-חלקיקים תאפשר לנו לכוון אותם על ידי הפעלת מתח חשמלי חיצוני ועל ידי כך להגביר את התכונות הלא לינאריות המקרוסקופיות של התערובת.

שתי קונפיגורציות ייצור מוצעות. מטרת שתיהן הינה לייצר מוליך גל ריבועי. הקונפיגורציה הראשונה הינה שיטת-הגשר שבה ליבת ה PFCB חווה איכול יוני ריאקטיבי (RIE). שיטה זו מהווה המשך של המתודולוגיה הקודמת שהוצעה במעבדה להתקנים פוטונים של ד"ר דן מרום, אולם מספר שיפורי מפתח בוצעו בשיטה זו.

הקונפיגורציה השנייה הינה שיטת-התעלות שבה רק Cytop חווה איכול. באמצעות שיטה זו ברצוננו למנוע חספוס שעלול להיווצר בשיטה החלופית עקב איכול של תערובת העשויה מ PFCB וננו-חלקיקים בו זמנית. בנוסף לא כל החומרים שמהם עשויים הננו-חלקיקים מורשים לשימוש בתוך תא האיכול מאחר והם עלולים לגרום לזיהומים במכונת האיכול. החלפת שיטת-הגשר עם שיטת-התעלה תתגבר ללא ספק על מכשול זה. אולם לכל אחת מהשיטות יש את האתגרים שלה. בעבודה זו ניסיתי להתגבר על כמה מהאתגרים ולייצר שיטה מהימנה והדירה לייצור מוליך גל פולימרי מתואם עם ננו-חלקיקים.

## **Table of content**

|  |    |
|--|----|
| <b>1. Introduction</b>   | 1  |
| <b>2. Theoretical background:</b>                                | 3  |
| 2.1 Rectangular waveguide  | 3  |
| 2.2 Nano crystals background and nonlinear composite             | 5  |
| 2.3 Polymer selection as the core and clad of the waveguide      | 7  |
| 2.3.1 PFCB as the core polymer                                   | 8  |
| 2.3.2 Cytop as cladding polymer                                  | 9  |
| 2.4 Adhesion of polymers   | 10 |
| 2.4.1 Coupling by chemical reaction                              | 11 |
| 2.4.2 Coupling polymers by interdiffusion                        | 11 |
| 2.4.3 Plasma surface treatment                                   | 11 |
| 2.4.4 Silane as adhesion promoter for polymer-substrate adhesion | 11 |
| 2.5 Fabrication method   | 12 |
| 2.6 Nonlinear waveguide theory                                   | 13 |
| <b>3. Waveguide characteristics</b>                              | 16 |
| 3.1 Height and width of the PFCB core                            | 16 |
| 3.2 Mode simulation  | 16 |
| 3.3 Mode confinement   | 17 |
| 3.4 Distance from the Silicon substrate                          | 18 |
| 3.5 Previous work  | 19 |
| <b>4. Waveguide fabrication</b>                                  | 21 |
| 4.1 General description  | 21 |
| 4.2 Preparation of the PFCB core material                        | 21 |
| 4.3 Ridge configuration waveguide                                | 25 |
| 4.3.1 Cytop adhesion to silicon                                  | 25 |
| 4.3.2 Cytop under-clad layer                                     | 25 |
| 4.3.3 PFCB core layer- adhesion to Cytop                         | 26 |
| 4.3.3.1 Silane mono layer  | 26 |
| 4.3.3.2 50nm thickness of SiO <sub>2</sub>                       | 26 |
| 4.3.3.3 100nm thickness PMMA                                     | 28 |
| 4.3.3.4 PFCB directly on Cytop                                   | 28 |

|  |           |
|--|-----------|
| 4.3.4 Etching Selectivity .....                                    | 30        |
| 4.3.5 Deposition of 50nm SiO <sub>2</sub> layer as hard mask ..... | 31        |
| 4.3.6 Lithography and development .....                            | 32        |
| 4.3.7 RIE .....  | 33        |
| 4.3.8 Cytop over clad .....  | 37        |
| 4.3.9 Glass cover .....  | 37        |
| 4.3.10 Dicing and polishing .....                                  | 38        |
| 4.4 Trench configuration waveguide.....                            | 38        |
| 4.4.1 5μm Cytop layer .....  | 39        |
| 4.4.2 Etching selectivity .....                                    | 39        |
| 4.4.3 50nm SiO <sub>2</sub> hard-mask .....                        | 40        |
| 4.4.4 Lithography and development .....                            | 41        |
| 4.4.5 RIE .....  | 42        |
| 4.4.6 Further optimization .....                                   | 44        |
| 4.4.7 PFCB filling .....   | 46        |
| 4.4.8 Cytop over-clad .....  | 47        |
| 4.4.9 Dicing and polishing .....                                   | 47        |
| <b>5. Summary and conclusions .....</b>                            | <b>49</b> |

## 1. Introduction

Nonlinear waveguides are a topic of research of great interest and importance. The high intensities in a single-mode guide and the long interaction length "open the door" for various nonlinear interactions at high efficiency such as self-phase modulation (SPM), cross-phase modulation (XPM) and stimulated Raman scattering. These effects can be exploited for several applications such as pulse compression and demultiplexing high bit-rate pulses [2]. More than anything else, the ability to design and control the properties of the waveguide itself makes it flexible and appropriate for promoting nonlinear effects.

In order to design a nonlinear waveguide there is a need to meet several requirements: the mode must be confined in the small core area in order to get high optical flux, the core must have nonlinear properties such as high order susceptibility according to the effect we would like to demonstrate and finally low losses are required.

Our long term goal is to design a nonlinear polymeric waveguide by using Cytop polymer for the cladding and PFCB polymer doped with nonlinear semiconductor nanocrystals (SC NCs) for the core, all operating in the optical telecommunication band (1.55 $\mu\text{m}$ ). In this way we use both the nonlinearity of the NCs which derive the properties from the bulk material and also the fabrication facilities for fabricating polymeric waveguide such as spin coating, photolithography, plasma ashing and reactive ion etching (RIE).

PFCB was chosen as the WG core since it has low loss of 0.29dB/cm in the optical communication regime, tunable refractive index (1.42-1.5) and has been demonstrated by Banin *et al* [3] a good host for the NCs. NCs usually consist of a crystalline semiconductor core surrounded by shell of a higher bandgap SC material. The shell provides the confining potential for the core electrons and protects it from the surroundings. The low polymerization temperature of PFCB material insures that the optical properties of the NCs will be minimally affected.

Cytop was chosen as the WG cladding since it has low loss of 0.022db/cm at the optical communication regime, high transparency and relatively low refractive index (1.34) [4] leading to high index contrast of  $\Delta n \sim 10\%$  to get a good confinement of the optical mode.

Former work in Dr. Marom laboratory included fabrication and characterization of a high index contrast linear polymeric waveguide made of Cytop and PFCB polymers. They reported on propagation loss of 1.06dB/cm at 1.55 $\mu\text{m}$  wavelength for a

1.5 $\mu$ m $\times$ 1.5 $\mu$ m square WG[1]. This high loss was obtained due to the roughness of the waveguide's side walls and fabrication imperfections of the waveguides.

In this work, one major effort was for improving the former fabrication process, improving on the reproducibility and reliability and making it compatible with the SC NCs to be embedded in the PFCB core.

These efforts also included optimization of the synthesized PFCB polymer. Especially the selection of the ratio of the two monomers composing the PFCB (TVE and BPVE), the % Wt. of the solution and the temperature of polymerization which was limited due to the NCs. Using two fluorinated polymers Cytop and PFCB introduced some problems in adhering between the two. Former work in Dr. Marom laboratory suggested using SiO<sub>2</sub> deposited in ICP CVD as an adhesive layer. However this solution introduces stress and complicates the process. In this work we suggest several alternative solutions for the adhesion problem. Furthermore we introduce a different flow leading to a "trench method" for fabricating a square polymeric waveguide. This method is also compatible with the NCs and allows us to choose several interesting NCs to be embedded in the PFCB core as oppose to the former ridge method in which some of the interesting materials were out of range.

## 2. Theoretical background:

### 2.1 Rectangular waveguide

Rectangular waveguides consist of a square or rectangular core surrounded by a cladding with lower refractive index (RI) than that of the core. The basic principle of wave guiding is based on total internal reflection (TIR) in which the optical beam is trapped within the core. This phenomenon can occur only if the RI of the core is higher than the RI of the cladding surrounding it [5].

Propagation within the waveguide is defined by wave equation, derived from Maxwell's equations:

$$\frac{\partial^2 H_y}{\partial x^2} + \frac{\partial^2 H_y}{\partial y^2} + (k^2 n^2(x, y) - \beta^2) H_y = 0 \quad (2.1)$$

Where  $\beta$  and  $k$  denote the propagation constant and the wave number respectively and  $H_y$  is the magnetic field when the dominant electric field is  $E_x$ .

The wave analysis we describe in this section for the rectangular waveguide is proposed by Marcantili [5] which assume that the electromagnetic field in the shaded core areas can be neglected (figure 2.1), since the electromagnetic field of the well-guided mode decays quite rapidly in the cladding region. The square waveguide core dimensions are  $2d \times 2d$ .

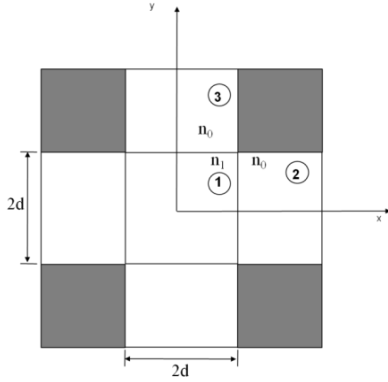


**Figure 2.1:** Three-dimensional rectangular waveguide

The solution for the above wave equation in each region is therefore:

$$H_y = \begin{cases} A \cos(k_x x - \phi) \cos(k_y y - \psi) & \text{region 1} \\ A \cos(k_x d - \phi) e^{-\gamma_x(x-d)} \cos(k_y y - \psi) & \text{region 2} \\ A \cos(k_x x - \phi) e^{-\gamma_y(y-d)} \cos(k_y d - \psi) & \text{region 3} \end{cases} \quad (2.2)$$

Where  $k_x, k_y$  are the transverse wave number and  $\gamma_x, \gamma_y$  are the decay

coefficients which should maintain:

$$\begin{cases} -k_x^2 - k_y^2 + k^2 n_1^2 - \beta^2 = 0 & \text{region 1} \\ \gamma_x^2 - k_y^2 + k^2 n_1^2 - \beta^2 = 0 & \text{region 2} \\ -k_x^2 + \gamma_y^2 + k^2 n_1^2 - \beta^2 = 0 & \text{region 3} \end{cases} \quad (2.3)$$

$$\Rightarrow \beta = \sqrt{k^2 n_1^2 - (k_x^2 + k_y^2)}$$

$\phi$  and  $\psi$  are the optical phases given by:

$$\begin{cases} \phi = (p-1) \frac{\pi}{2} & (p = 1, 2, \dots) \\ \psi = (q-1) \frac{\pi}{2} & (q = 1, 2, \dots) \end{cases} \quad (2.4)$$

By applying the boundary conditions for the electric field  $E_z$  at  $x=d$  and for the magnetic field  $E_{pq}^x$  at  $y=d$  we obtain the following dispersion equation:

$$k_x d = (p-1) \frac{\pi}{2} + \tan^{-1} \left( \frac{n_1^2 \gamma_x}{n_0^2 k_x} \right) \quad (2.5)$$

$$k_y d = (q-1) \frac{\pi}{2} + \tan^{-1} \left( \frac{\gamma_y}{k_y} \right) \quad (2.6)$$

A similar derivation for the dominant electric field propagation along  $\hat{y}$  (i.e.  $E_y$ ) leads to:

$$k_x d = (p-1) \frac{\pi}{2} + \tan^{-1} \left( \frac{\gamma_x}{k_x} \right) \quad (2.7)$$

$$k_y d = (q-1) \frac{\pi}{2} + \tan^{-1} \left( \frac{n_1^2 \gamma_y}{n_0^2 k_y} \right) \quad (2.8)$$

Figure 2.2 presents the first four modes in a  $4\mu\text{m} \times 4\mu\text{m}$  dimensions waveguide with an index contrast of 10%.

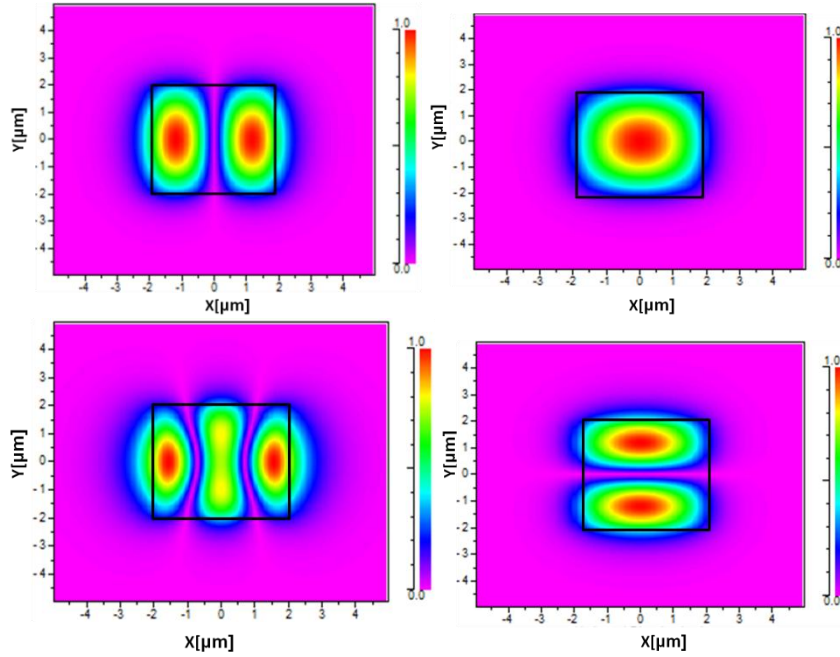


**Figure 2.2** : First four modes of a  $4\mu\text{m} \times 4\mu\text{m}$  dimensions waveguide with an index contrast of 10%.

## 2.2 Nano crystals background and nonlinear composite

Semiconductor (SC) colloidal nanocrystals are very attractive for light-interacting applications, including light-emitting diodes [6], and lasing [7], due to their size-controlled spectral tunability and chemical flexibility. In our case we would like to use the SC NCs as dopands in the PFCB core in order to produce a nonlinear waveguide.

The properties of SC NCs are governed by their bulk crystalline properties that are altered by their shape and physical confinement. This assumption is valid as long as the physical size of the NCs is not lower than the Bohr radius of the bulk exciton  $a_{exciton}$  influenced by Bohr radius (derived for hydrogen), the rest mass of the electron, the permittivity of the bulk material and the reduced mass of the electron and hole effective masses in the bulk material [8]. Otherwise quantization of the energy levels is caused and hence increases the effective bandgap. Control over the size and shape of colloidal NCs is accomplished by simple control over the supply of precursors and thermal conditions during the chemical reactions that govern their growth.

Figure 2.3 summarizes the bandgap size of different SC quantum dots (QDs, i.e. sphere NCs) [9]. One can clearly see that some of the materials possess active properties in optical telecommunications wavelength of interest, i.e. InAs, PbS, PbSe,

etc. Other NCs are interesting due to their permanent dipole moment (i.e., CdSe) [10] which can assist an external electric field to orient them and thus enhance the nonlinear response of the whole composite.

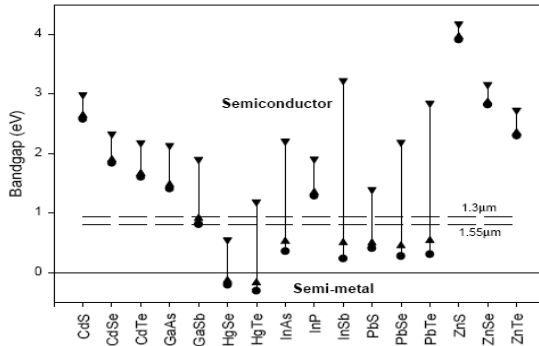


**Figure 2.3:** Sensitivity of bandgap energies to particle size for a range of semiconductors. Bandgaps are shown for the bulk forms (circles) and at dot radii of 10nm (up triangles) and 3nm (down triangles)

The synthesis of the SC NCs can be subdivided to two steps involved; the preparation of the colloidal SC NCs and the application of a capping molecules and/ or shelling layer. The shell, which consists of SC material with a higher bandgap, provides the confining potential for the core electrons along with passivating and protecting it from the surroundings. It also reduces the effects of surface states.

The shell is capped by organic ligands that give the NCs their solubility and prevent aggregation.

Growing NC in the shape of nanorods (NRs) increases the optical cross-section, and adds polarization dependence to its optical interactions [11,12].

The synthesis procedure can produce large NC quantities, and the NCs can be stored until needed for further processing in the colloidal state. The nanocrystals are dispersed into the PFCB and the entire composite can be treated as a new material, provided that the NCs are much smaller than the optical wavelength of the electric field propagating through the composite ( $\lambda$ ) and that the NCs' typical size ( $a$ ) is much smaller than the distance between them ( $b$ ). According to Maxwell-Garnet model we can treat the composite as a continuum regarding the electric field of the optical wave (figure 2.4)[13]. In other words we can relate the composite as a homogenous material which has an effective permittivity and effective NL susceptibilities depending on the materials it is composed of.

$$\langle \vec{D} \rangle = \vec{\epsilon}_{eff} \langle \vec{E} \rangle + \epsilon_0 \chi_{eff}^{(2)} \langle \vec{E} \rangle^2 + \epsilon_0 \chi_{eff}^{(3)} \langle \vec{E} \rangle^3 \quad (2.9)$$

It should be noted that although the Maxwell-Garnet model deals with metal inclusions, it can be also be used to treat dielectric ones [14].

The significance of the composite that the NCs can be synthesized and engineered with desirable optical properties, while the polymer waveguides can be independently optimized for optical fiber mode matching and utilize simplified fabrication.

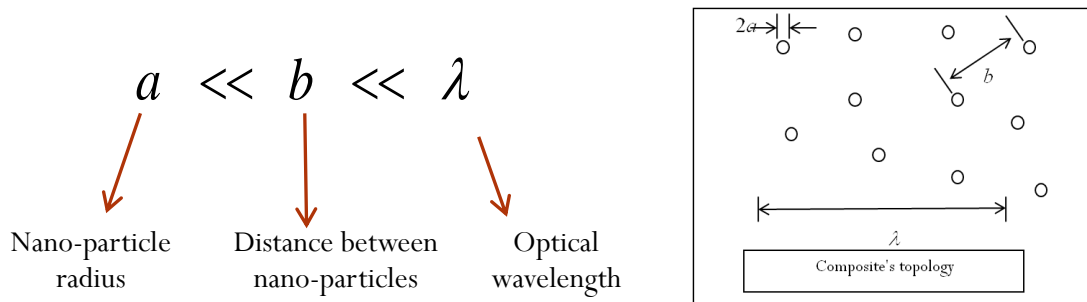


**Figure 2.4:** Composite topology due to Maxwell-Garnet model conditions

### 2.3 Polymer selection as the core and clad of the waveguide

Organic polymers can replace inorganic materials in many photonic devices since they offer low-cost fabrication, adequate transparency in the visible and near-infrared spectra, and versatility in structures making it flexible in design. Fluorinated polymers in particular have low moisture absorption, good optical stability after thermal aging and typically low propagation loss at telecommunication wavelengths.

Removing hydrogen and replacing it with fluorine in the organic network negates absorption due to the C-H bonds that have strong absorption in the visible and near infrared regions which is where most communication systems operate. The substitution of hydrogen atoms by fluorine decreases optical losses because the wavelengths of the fundamental stretching vibrations of C-F bonds are 2.8 times larger than that of the C-H bond [15].

Therefore fluoropolymers are well suited for wave guiding IR light presenting very low absorption ( $<0.15\text{dB/cm}$ ) over the range of 400-1600nm, offer high temperature stability and long durability and can be patterned using standard spin-coating, lithography and etching procedures. However, most fluoropolymers do not exhibit adequate solubility in common solvents making it difficult in planar structures processes.

### 2.3.1 PFCB as the core polymer

The polymer investigated in this work is Perfluorocyclobutyl (PFCB) (Tetramer Technologies, Inc.) which is comprised of two monomers that can be dissolved in a variety of solvents such as Mesitylene, Toluene, and Chloroform.

In our research PFCB functions as the waveguide core since it has been proven as a suitable host for nanocrystals [3]. It is also compatible with the nanocrystals constraints of having low temperature of polymerization of 150°C. Doping the PFCB core with nanocrystals will provide a nonlinear response to the composite.

PFCB comprises a family of partially fluorinated copolymers with selectable refractive index of 1.42-1.5 based on copolymer composition, and also selectable glass transition temperatures (130°C-350°C).

John Ballato showed optical properties of PFCB composed of different monomers ratio [16,17,18].

Figure 2.5 shows the measured transmission spectrum for one type of PFCB composed of TVE monomer. This spectrum is according to Ballato's research and based on calculated attenuation due to harmonic vibrations of C-H, C-O and C-F bonds in the PFCB polymer. As can be seen, PFCB exhibits below 1db/cm in the visible and near IR and therefore is a good candidate for the core waveguide.

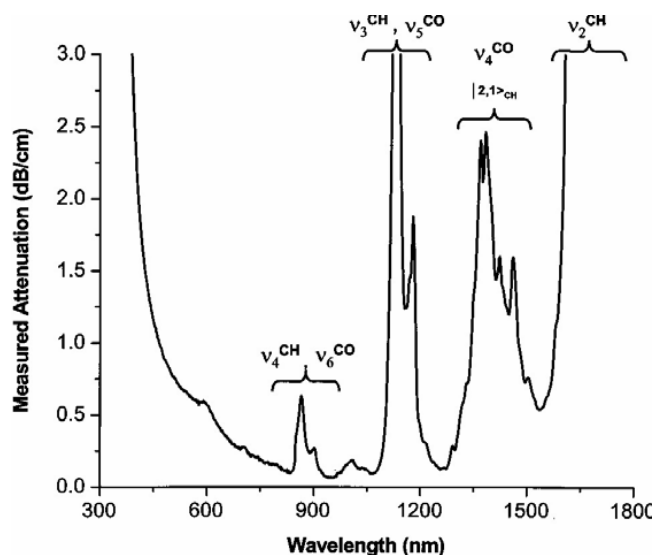
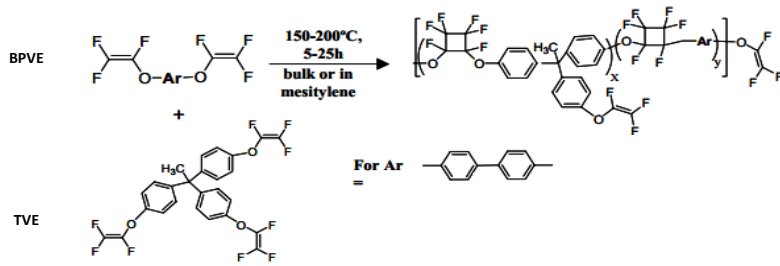


Figure 2.5: Measured attenuation Vs. wavelength for TVE PFCB

In our research we synthesize PFCB using TVE and BPVE monomers (figure 2.6).



**Figure 2.6:** Copolymerization of BPVE and TVE monomers.

We examined two ratios of TVE:BPVE, (1:9) and (1:1). The glass transition temperature of TVE is 350°C and 165°C for BPVE [17], therefore the calculated  $T_g$  for the entire solution derived from the equation:

$$\frac{1}{T_g} = \frac{\% \text{ monomer } 1}{T_{g1}} + \frac{\% \text{ monomer } 2}{T_{g2}} \quad (2.10)$$

is 174°C and 224 °C for (1:9) and (1:1) ratios respectively.

The refractive index according to figure 2.7 is between 1.49 to 1.5 for 1550 nm wavelength [19], and depends on the relative monomers ratio.

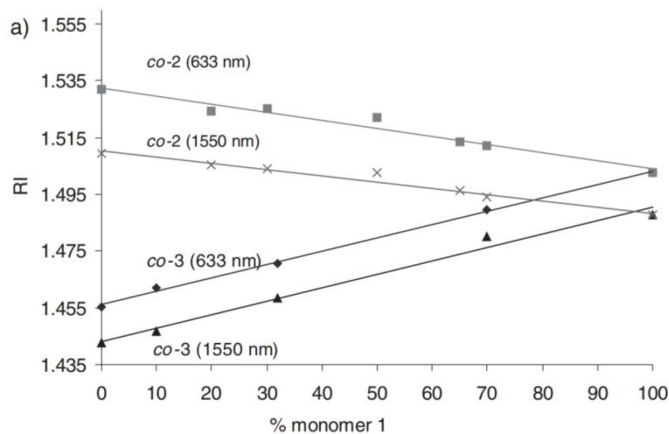


**Figure 2.7 :** Refractive index Vs. copolymer compositions for TVE (monomer 1) and BPVE (monomer 2)

### 2.3.2 Cytop as cladding polymer

For the cladding material, we chose Cytop polymer (Bellex International Corporation). Cytop has an amorphous (non-crystalline) structure unlike conventional fluoropolymers (figure 2.8). This makes CYTOP exceptionally transparent in the near IR, with visible light transmission levels greater than 95% and low loss of 0.022db/cm for 1.55μm wavelength.

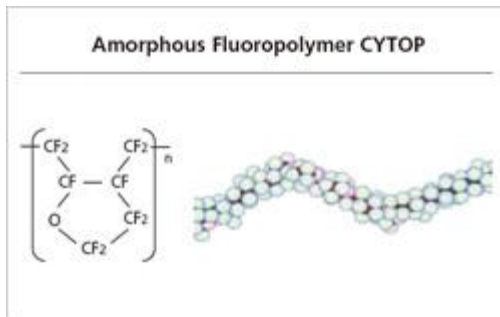


**Figure 2.8:** Chemical structure of Cytop polymer

Figure 2.9 shows Cytop transmittance vs. wavelength in 200-2000nm spectral range. It can be seen that Cytop has indeed around 95% of transparency in 1500nm wavelength and consequently can be used for optical communication applications.

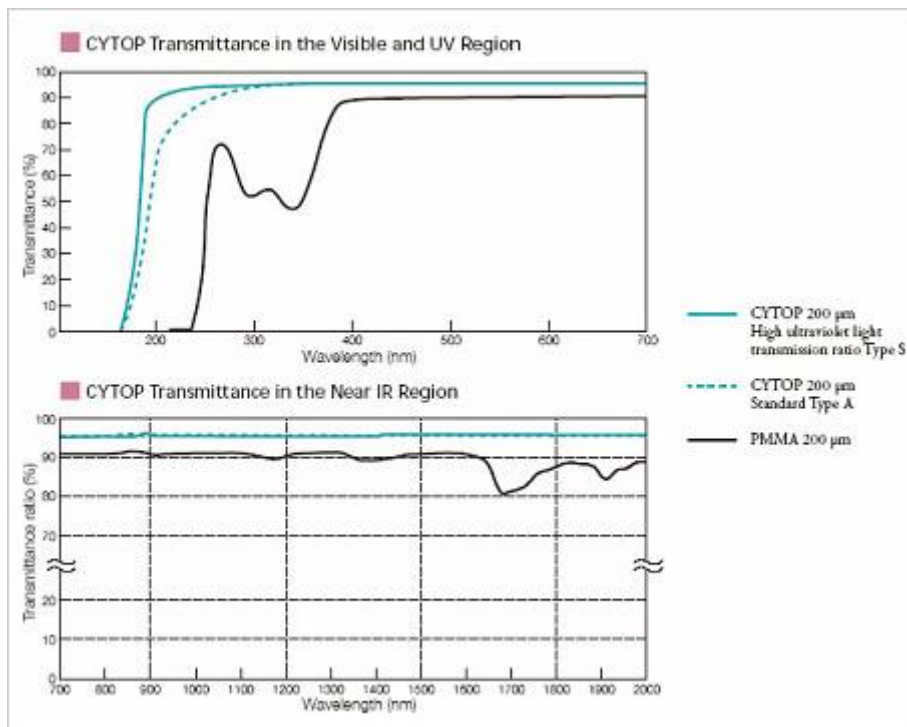


**Figure 2.9:** Cytop transmittance vs. wavelength in a range of 200-2000nm

Cytop can be dissolved in a special fluorinated solvent and applied using a variety of coating methods. Cytop has a 1.34 refractive index. Therefore the waveguide has a high index contrast  $\Delta n$  of  $\sim 10\%$  which allows highly confined optical mode operation. Cytop glass transition temperature is  $108^{\circ}\text{C}$ . However, adhering PFCB to Cytop is not an easy task. In our research we examined different methods to couple the two. From using an external material as a coupling agent to direct adhesion of the two polymers.

#### 2.4 Adhesion of polymers

In order to form a strong polymer-polymer adhesion it is necessary for the network of the polymer to be continuous across the interface. This continuity can be formed by either chemical reaction, chain interdiffusion, if the materials are sufficiently

miscible, the use of coupling chains placed at the interface or by plasma surface treatment.

Polymer-Silicon substrate adhesion also requires special treatment. Here Silane as adhesion promoter is suggested.

#### **2.4.1 Coupling by chemical reaction**

A common technique to couple between two bulk polymers is to introduce into one or both of the materials a small percentage of chemically modified chains that can react with the other polymer to form coupling chains at the interface.

A classic example of this method is to couple polypropylene by maleic anhydride grafted polypropylene chains using Nylon 6. However, this adhesion between the polymers can fail either by pullout or scission of these coupling chains.

Pullout at low forces can occur if either one of the blocks in the coupling copolymer is rather short or if there are too many coupling chains at the interface.

#### **2.4.2 Coupling polymers by interdiffusion**

It is possible to couple two polymers by chain interdiffusion if they are miscible in each other, or at least sufficiently miscible to form a broad interface.

Welding is the most common way to couple polymers by interdiffusion. Polymer diffusion normally occurs by the process of reptation where very long linear entangled molecules move in a snake-like thermal motion in a polymer solution.

Therefore interface coupling is achieved by a chain end initially crossing the interface and then the rest of the chain slowly follows it across. Here also chain pullout is expected after short jointing time [20].

#### **2.4.3 Plasma surface treatment**

A number of applications of plasma involve the surface treatment of plastic materials, prior to coupling another layer. An example is the treatment of reinforcing fibers that are to be integrated into an epoxy structure. Treatment in an oxygen plasma increases surface roughness. These pitted fibers enhance adhesion and a good mechanical bond is produced with enhanced rigidity and strength.

Plasma processing of plastics can also convert a hydrophobic surface to a hydrophilic surface. This type of treatment usually requires short exposure (3-5 minutes) at low power [21].

#### **2.4.4 Silane as adhesion promoter for polymer-substrate adhesion**

Silane coupling agents have the ability to form a durable bond between organic and inorganic materials. It has a general chemical formula of the form:



The general formula of Silane coupling agent typically shows the two classes of functionality.  $X$  is a hydrolyzable group typically alkoxy, acyloxy, halogen or amine. Following hydrolysis (the cleavage of chemical bonds by the addition of water), a reactive silanol group is formed, which can condense with other silanol groups, for example, those on the surface of siliceous fillers, to form siloxane linkages. The  $R$  group is a nonhydrolyzable organic radical that may possess a functionality that imparts desired characteristics.

Reaction of Silane involves four steps. Initially, hydrolysis of the three labile groups occurs. Condensation to oligomers follows (a molecule that consists of a few monomer units). The oligomers then hydrogen bond with OH groups of the substrate. Finally during drying or curing, a covalent linkage is formed with the substrate with concomitant loss of water. Although described sequentially, these reactions can occur simultaneously after the initial hydrolysis step. At the interface, there is usually only one bond from each silicon of the organosilane to the substrate surface. The two remaining silanol groups are present either in condensed or free form. The  $R$  group remains available for covalent reaction or physical interaction with other phase [22].

Figure 2.10 shows a brief scheme of silane deposition

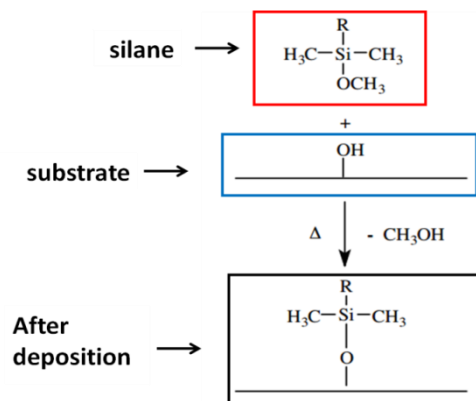


**Figure 2.10** : Schematic figure of silane deposition

## 2.5 Fabrication methods

Choosing polymers as the waveguide core and clad enables us to use known techniques in the microelectronic technology making it easy to fabricate[23].

In this research several fabrication tools were used.

Since the polymers we use are miscible we can use spin coating in order to get a uniform layer at the desired thickness.

The SiO<sub>2</sub> adhesive layer and hard mask were deposited using plasma enhanced chemical vapor deposition (PECVD).

The photolithography was carried out in MA6 mask aligner using AZ1505 as positive photoresist and Ma-N as negative photoresist.

The etching of the features was carried out using reactive ion etching (RIE) machine with O<sub>2</sub> for *polymer etch* and CHF<sub>3</sub> and Ar for *SiO<sub>2</sub> etch*.

And finally the adhesion between the Cytop over-clad and the protective glass was done by using Norland UV glue.

The inspection machines we used were: Nuclear Magnetic Resonance spectroscopy (NMR) in order to determine the degree of polymerization of the PFCB polymer before and after curing, Scanning Electron Microscope (SEM) in order to determine the waveguide dimensions, Optical Reflectometer in order to determine the width of the layers, Elipsometer in order to determine the width of the layers and also the refractive index of the PFCB material and finally Mechanical and Optical Profilometer in order to follow and control RIE step and also observe surface roughness.

## 2.6 Nonlinear waveguide theory

Our long term goal is to produce a waveguide with an enhanced NL response. This can be achieved by using a composite of PFCB and NCs for wave guiding in the core waveguide. Fabricating such a waveguide will allow us to create active and/or nonlinear optical devices operating in the near-IR, and to demonstrate that they offer similar, and sometimes unique, functionality to that of the epitaxial approach. The epitaxial growth approach is well understood and developed, and dominates the photonic component marketplace. But the fabrication facilities are costly to install, maintain, and operate, and the production process consists of many time consuming steps, all leading to the high cost of photonic components. Alternatively, planar fabrication procedures allows for a novel approach toward realizing simpler integration of NCs into optical devices.

The wave equation for nonlinear materials is given by [2]:

$$\nabla^2 \vec{E} - \frac{1}{c^2} \frac{\partial^2 \vec{E}}{\partial t^2} = \mu_0 \frac{\partial^2 \vec{P}_L}{\partial t^2} + \mu_0 \frac{\partial^2 \vec{P}_{NL}}{\partial t^2} \quad (2.12)$$

Where  $\vec{P}_L$  denotes the linear term of the polarization and  $\vec{P}_{NL}$  is the nonlinear polarization, which for centrosymmetric materials do not have  $\chi^{(2)}$  response:

$$\vec{P}_L = \epsilon_0 \chi^{(1)} \vec{E} \quad (2.13)$$

$$\vec{P}_{NL} = \chi^{(3)} [\vec{E} \cdot \vec{E}^*] \vec{E}$$

The nonlinear Schrödinger equation is derived from Eq. (2.12) and describes the pulse envelope propagation (A):

$$\frac{\partial A}{\partial z} + \beta_1 \frac{\partial A}{\partial t} + j \frac{\beta_2}{2} \frac{\partial^2 A}{\partial t^2} + \frac{\alpha}{2} A = j\gamma |A|^2 A \quad (2.14)$$

Where the left hand term of the equation refers to the linear terms and includes  $\beta_1$  which is the inverse of the group velocity,  $\beta_2$  which represent the chromatic dispersion of the material and  $\alpha$  which represent the absorption or gain of the material.

The right hand term refers to the nonlinearity of the material represented by  $\gamma$  [23]:

$$\gamma = \frac{3\omega \cdot \epsilon_0 Z_0^2}{4n_{core}^2 A_{eff}} \chi^{(3)} \quad (2.15)$$

where  $Z_0$  is the impedance of the vacuum:  $Z_0 = \sqrt{\mu_0/\epsilon_0} = 377\Omega$ ,  $\omega$  is the optical frequency of the propagating wave,  $n_{core}$  is the linear RI of the nonlinear composite of PFCB and NCs,  $\chi^{(3)}$  is the effective susceptibility which is influenced by the composite materials and the geometry of the NCs and  $A_{eff}$  is the effective modal area which measure the quality of the confinement of the mode and is given by [24]:

$$A_{eff} = \frac{Z_0^2}{n_{core}^2} \frac{\left| \int_{A_{co}} \text{Re} \{ \vec{E}(x, y) \times \vec{H}^*(x, y) \} \vec{e}_z dA \right|^2}{\int_{A_{core}} |\vec{E}(x, y)|^4 dA} \quad (2.16)$$

A good confinement of the optical mode in the core region leads to greater expression in the denominator resulting in a smaller  $A_{eff}$  and higher nonlinear coefficient  $\gamma$ .

Yedidya from Dr. Marom's research team analyzed the NL response of a composite composed of PFCB as the host material and CdSe nanorods as the inclusions both for the case of aligned and randomly oriented nanorods[25]. The properties of the

nanorod were:  $12 \times 120 \text{ nm}$  (W×L) nanorods dimensions, polymerization temperature of  $T=150^\circ\text{C}$  and volume fraction of  $p=4\%$ . For randomly oriented nanorods, the calculated  $A_{eff}$  for a square  $1.5 \times 1.5 \mu\text{m}^2$  core dimensions was  $2.7 \mu\text{m}^2$ . The third order NL susceptibility reported in Yedidya's thesis was:  $\chi_{eff}^{(3)} / \chi_{CdSe}^{(3)} = 2.25\%$  along the  $\hat{x}$  direction.

For a random oriented composite described above with the minimum  $A_{eff}$ , the maximum calculated NL coefficient was  $\gamma = 68 (W \cdot m)^{-1}$ . For comparison glasses based NL optical fibers achieve maximum values of  $\gamma = 50 (W \cdot m)^{-1}$ .

It is important to mention that there is another degree of freedom for enhancing  $\gamma$  achieved by applying electric voltage on the nanorods and aligning them along the electric field direction.

In this way we can achieve enhanced NL coefficient of  $\gamma = 119 (W \cdot m)^{-1}$  with a  $10^6 \text{ V/m}$  aligning electric field, along the optical field direction.

### 3. Waveguide characteristics

This chapter presents the design and analysis of a high index contrast (HIC) single-mode waveguide in highly confined geometries constructed in PFCB polymer using Cytop as the outer cladding material. The calculations were done under the assumption that the RI of PFCB is not affected by the RI of the nanocrystals, which is reasonable for low volume fractions.

The simulations were carried out in Rsoft and Comsol multiphysics software packages which use numerical analysis techniques.

#### 3.1 Height and width of the PFCB core

In order to achieve a single mode waveguide with PFCB's RI of 1.5 and 1.34 of Cytop the square WG core should have  $1.7\mu\text{m}\times 1.7\mu\text{m}$  dimensions.

Figure 3.1 presents the electric fields of square waveguides at  $1.7\mu\text{m}\times 1.7\mu\text{m}$  and  $1.8\mu\text{m}\times 1.8\mu\text{m}$  dimensions. It can be seen that only in the case of  $1.8\mu\text{m}\times 1.8\mu\text{m}$  waveguide dimensions, the second mode arises.

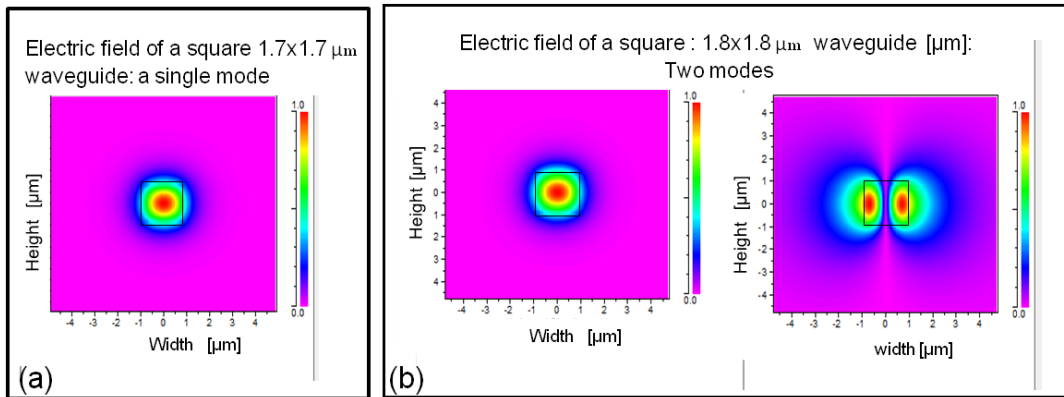


**Figure 3.1:** a. Electric field of  $1.7\mu\text{m}\times 1.7\mu\text{m}$  waveguide dimensions  
b. Electric field of  $1.8\mu\text{m}\times 1.8\mu\text{m}$  waveguide dimensions

In order to reduce polarization effects, which occur when the waveguide core is not a symmetric one, we chose square waveguide geometry. Using the above information, we decided the dimensions of the core to be  $1.5\mu\text{m}\times 1.5\mu\text{m}$ .

#### 3.2 Mode simulation

In order to achieve a single mode waveguide with good mode confinement, the effective index of the waveguide should be above Cytop ( $n=1.34$ ). The mode profile simulations have been performed in Comsol 4, a 2-D mode solving simulation program. Figure 3.2 shows the simulated results for a  $1.5\mu\text{m}\times 1.5\mu\text{m}$  square waveguide, where the mode intensity profile has been calculated for TE incident wave (the TM intensity mode profile is identical). Figure 3.3 shows the simulated results for

rectangular waveguide with core dimensions of  $0.85\mu\text{m} \times 1.5\mu\text{m}$ , where the mode intensity profile has been calculated for both TE and TM incident waves.

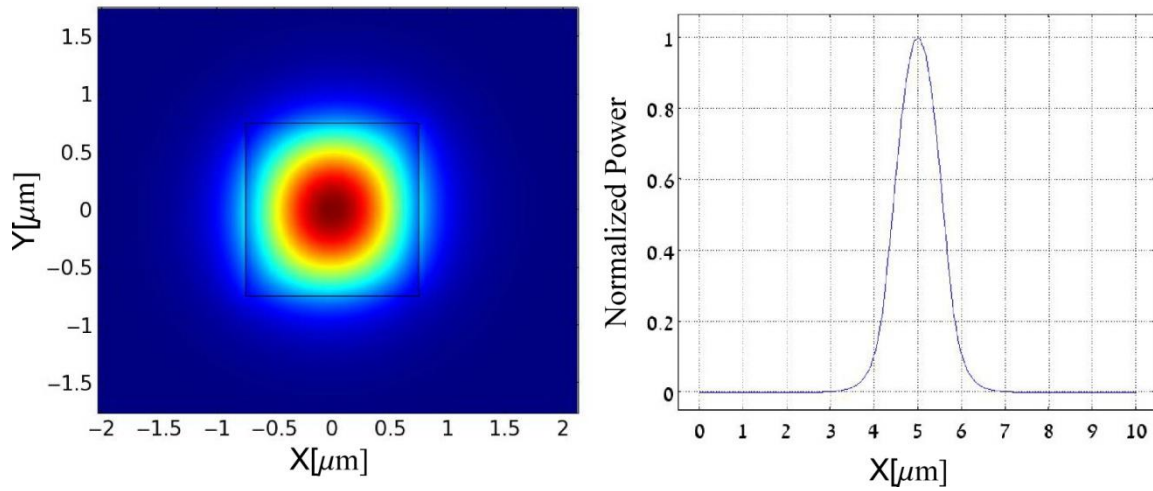


**Figure 3.2:** Simulated TE intensity mode profile result for  $1.5\mu\text{m} \times 1.5\mu\text{m}$  square waveguide with a  $1.88\mu\text{m}$  waist.

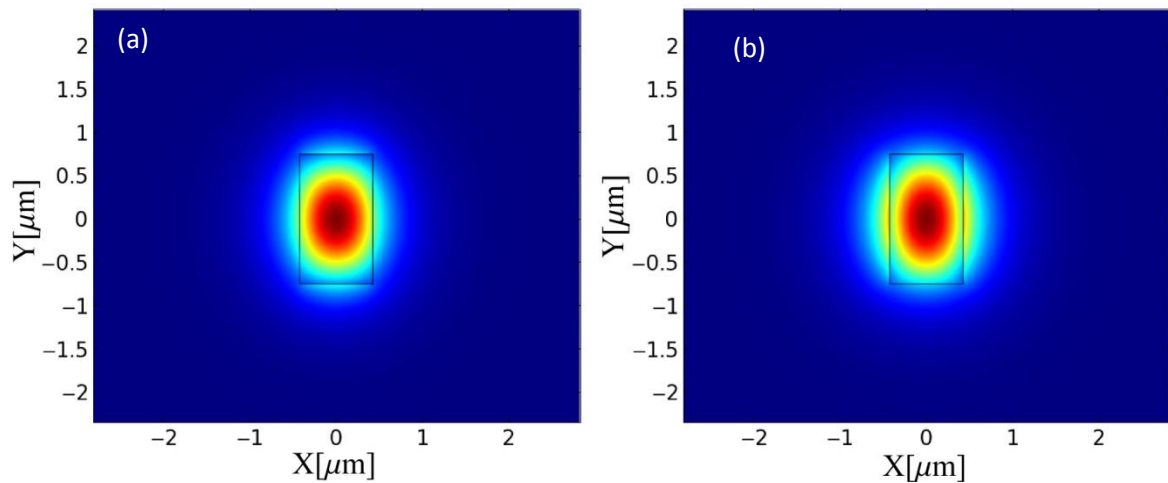


**Figure 3.3:** Simulated TE(a) and TM(b) intensity mode profile results for  $0.85\mu\text{m} \times 1.5\mu\text{m}$  rectangular waveguide with a  $1.906\mu\text{m} \times 2.06\mu\text{m}$  waist.

### 3.3 Mode confinement

The confinement factor is defined as the ratio of the power in the core to the total power propagating through the waveguide. The confinement factor is therefore given by [5]:

$$\Gamma = \frac{P_{core}}{P_{core} + P_{clad}} \quad (3.1)$$

The more  $\Gamma$  tends to one, the better confinement of the mode is achieved.

$P$  is the power defined by:

$$P = \int_{-\infty}^{\infty} \vec{S} \cdot \hat{Z} \, dx dy \quad (3.2)$$

Where  $\vec{S} \cdot \hat{Z}$  is the projection of Poynting vector over the direction of the wave propagation.

The Poynting vector is given by:  $\vec{S} = \frac{1}{2} \text{Re}\{\vec{E}X\vec{H}^*\}$  (3.3)

And represent the directional energy flux density of an electromagnetic field.

The modal confinement is related to the effective index. For a given core and cladding materials, the higher the effective index is, the more confined the mode is. Therefore the fundamental mode tends to be the most confined just as it tends to have the highest effective index.

The confinement factor of the fundamental mode calculated by Eq.( 3.1) of a 1.5 $\mu\text{m}$ X1.5 $\mu\text{m}$  waveguide core at a wavelength of 1550nm is approximately  $\Gamma = 0.56$  and  $\Gamma = 0.47$  for 0.85 $\mu\text{m}$ X1.5 $\mu\text{m}$  waveguide core (as calculated with Comsol 4 software).

Related to the modal confinement is the spot size (beam radius) of the propagating field and the optical intensity. High confinement in a small core waveguides means high intensity necessary for NL effects. The spot size of a 1.5 $\mu\text{m}$ X1.5 $\mu\text{m}$  waveguide core at a wavelength of 1550nm is approximately 1.88 $\mu\text{m}$  as shown in figure 3.2 ( $e^{-2}$  waist of the power density), when making a Gaussian approximation [26]. This means the average optical intensity for 0dBm input power is approximately :

$$I = \frac{P}{\pi w^2} = 9 \times 10^3 \frac{W}{\text{cm}^2} \quad (3.4)$$

### 3.4 Distance from the Silicon substrate

The devices we design are fabricated in a planar form where the substrate is a silicon wafer. Therefore there is a chance that there will be a leakage of the confined optical mode to the silicon substrate due to its high refractive index (3.48). That means that losses will occur. The leakage of the optical mode can occur when the low index under-cladding is too thin.

In order to determine the sufficient thickness of the Cytop under-cladding, several thicknesses were simulated. Figure 3.4 shows the losses of the core waveguide taking different thicknesses of Cytop under-clad from 0.5 $\mu\text{m}$  to 3.5 $\mu\text{m}$ . As can be seen, the thicker the under-clad layer, the less lossy the waveguide is due to leakage to the Silicon substrate. We decided to take 3.5 $\mu\text{m}$  under-clad thickness.

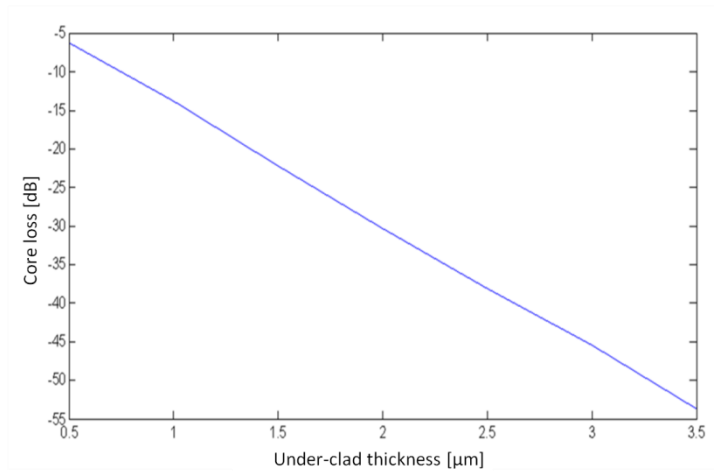


**Figure 3.4:** The substrate leakage loss vs. under-clad thickness computed by consol mode solving simulation program for 0dBm input power.

Figure 3.5 demonstrate the intensities of the fundamental mode of  $1.5\mu\text{m}\times 1.5\mu\text{m}$  core dimension waveguide of two extreme  $0.35\mu\text{m}$  and  $3.5\mu\text{m}$  under-clad thicknesses. The leakage to the silicon substrate can be clearly seen in the case of  $0.35\mu\text{m}$  thickness.

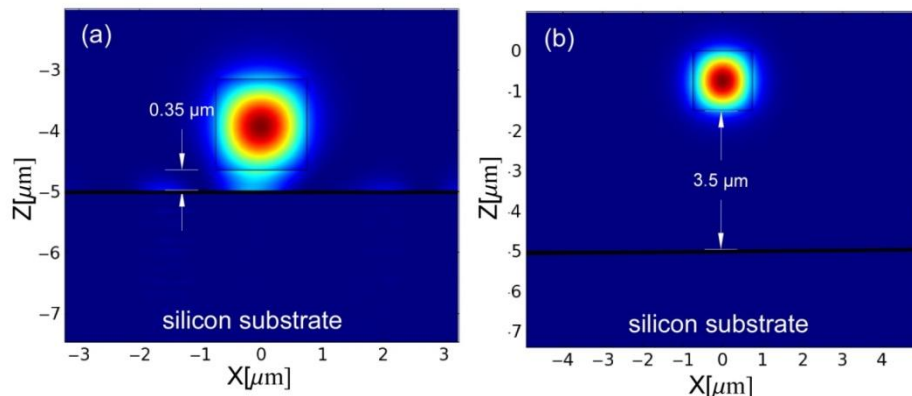


**Figure 3.5:** Intensity of the fundamental mode of  $1.5\mu\text{m}\times 1.5\mu\text{m}$  waveguide dimensions.

- a.  $0.35\mu\text{m}$  distance from the silicon substrate
- b.  $3.5\mu\text{m}$  distance from the silicon substrate

### **3.5 Previous work**

Previous work done in Dr. Marom's laboratory dealt with high contrast polymer waveguide consisting of Cytop as the waveguide cladding and PFCB as the waveguide core [1]. The synthesis of the PFCB included 1:1 monomers ratio (TVE: BPVE) diluted in Mesitylene solvent for receiving 60 %Wt. solution.

A  $3.5\mu\text{m}$  Cytop under-clad layer thickness, cured in the oven set to  $120^\circ\text{C}$  for 4 hours.

In order to couple Cytop to PFCB a  $30\text{nm}$   $\text{SiO}_2$  layer in ICP RIE was deposited in

40°C deposition temperature. 1.5 $\mu\text{m}$  PFCB core layer, cured in the oven set to 120°C for 16 hours. Another 30nm SiO<sub>2</sub> adhesive layer and finally a 3.5 $\mu\text{m}$  Cytop over-clad layer. Figure 3.6 shows the cross section of the waveguide structure:

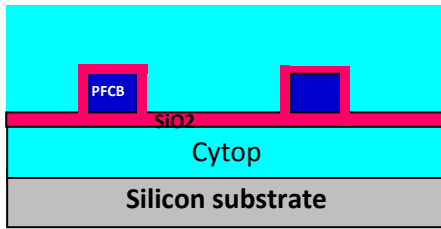


**Figure 3.6:** A cross section of high contrast waveguide fabricated in the previous work

The results after measuring:

A Gaussian fit mode size height of  $2\omega_0=2.75\pm 0.4\mu\text{m}$  and width of  $2\omega_0=2.88\pm 0.42\mu\text{m}$  as shown in figure 3.7b

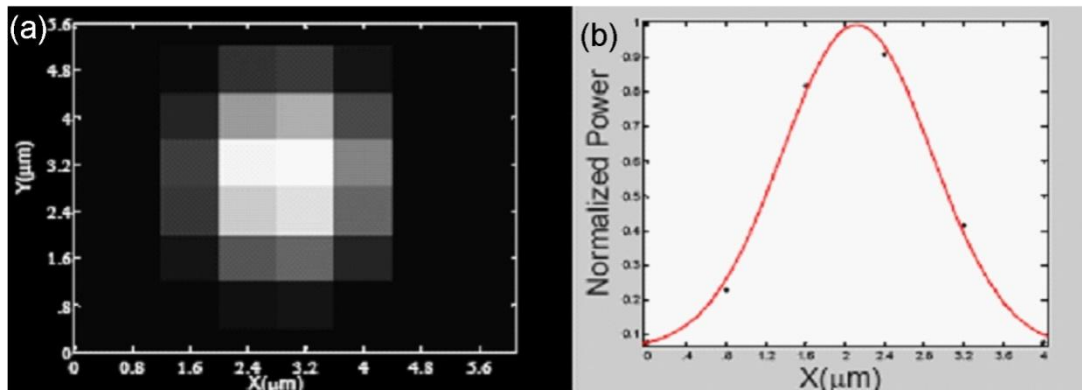


**Figure 3.7:** a. Image of waveguide output with dimensions of 1.5 $\mu\text{m}$  X1.5 $\mu\text{m}$ . b. Intensity profile with Gaussian fit which gives width of  $2\omega_0=2.88\pm 0.42\mu\text{m}$ .

Propagation loss of 1.06dB/cm was measured for 1.5 $\mu\text{m}$ x1.5 $\mu\text{m}$  waveguide dimensions and 0.851cm waveguide length.

In addition bend loss of 0.23dB/90<sup>0</sup> was measured for TM polarization and 0.2dB/90<sup>0</sup> for TE polarization for 1.5 $\mu\text{m}$ x1.5 $\mu\text{m}$  waveguide dimensions for rings with radius bend R=350 $\mu\text{m}$ .

Those high losses were due to residual surface roughness on the etched sidewalls and fabrication imperfections of the waveguides.

Several improvements were carried out in my research in order to achieve lower losses and to produce a reliable and reproducible fabrication method.

I also tried to design a process which will be compatible with the NCs to be embedded in the PFCB core.

## 4. Waveguide fabrication

### 4.1 General description

As previously mentioned, the main objective of this work is to improve the previous fabrication process of waveguide structures with a PFCB polymer as core, which we synthesize ourselves, and Cytop polymer as cladding, making the process reproducible and reliable.

Furthermore, we would like to design a process that will be compatible core-doping the PFCB with SC nanocrystals. Figure 4.1 presents the device structure with and without nanocrystals (b and a respectively)

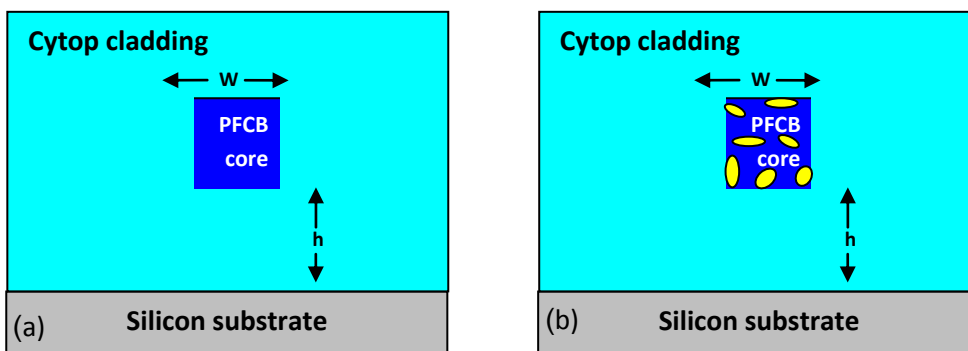


**Figure 4.1:** Device structure (a) without nanocrystals (b) with nanocrystals in the PFCB core

The developed process flow proved more challenging than expected. Both materials are fluorinated polymers therefore presenting adhesion problems. We also had to face difficulties of cracks and stresses since the polymerization temperature of PFCB is 150°C as oppose to our previous research when we cured at 120°C due to cracks that appeared in the Cytop-SiO<sub>2</sub>-PFCB structure. The cracks appeared because of CTE mismatch of the materials; (~74 ppm/C° for Cytop, ~0.5 ppm/C° for SiO<sub>2</sub> and ~60 ppm/C° for PFCB)

Developing a reliable and reproducible technique for PFCB synthesis was not an easy task. We had to take into account the desired width of the PFCB layer, the material degree of polymerization before and after spin coating and the material transparency.

### 4.2 Preparation of the PFCB core material

PFCB is a fluorinated polymer which is composed of two monomers TVE and BPVE. Different ratio of the monomers will affect the refractive index, the material viscosity, the potential degree of polymerization, and the glass transition temperature ( $T_g$ ). The solvent we use is Mesitylene. Different %Wt. of the solution will affect both the

viscosity of the material which is important for setting the layer thickness, and the duration of the process. The polymerization process is a radical one in which heating the solution create free radicals which link to one another to create the chain polymer with the TVE and BPVE monomers building blocks organized randomly.

We have examined two different ratios: 1:1 and 1:9 (TVE: BPVE) and several %Wt. of solutions.  $\left(\frac{\text{monomers}}{\text{monomers}+\text{solvent}}\right)$ .

The synthesis had to be carried out in an inert environment to prevent oxidation. Therefore all the tools we used for the polymer synthesis were cleaned and dried from water during the process. The solvent also had to be thoroughly dried which was achieved by using molecular sieves. In order to apply a successful spin coating, around 45% degree of pre-polymerization was required.

TVE and BPVE monomers (1:1 or 1:9) diluted in Mesitylene solvent (40%-60% Wt.) were inserted into a clean and dry 3 necks flask. A magnetic stirrer was also inserted inside the flask and it was then sealed with septums while a Nitrogen needle was bubbling in it. The middle neck of the flask was connected to a condenser to avoid solvent evaporation. The flask was put into an oil bath.

We stirred the solution and heated it to 60°C for half hour duration in order to make sure no Oxygen was in it. The polymerization was carried out in a temperature of 160°C. The duration of polymerization was different for different solutions, depending on both the ratio of the monomers and the %Wt. of the solution. When the process came to an end, an integrated NMR check was carried out in order to determine the solution degree of polymerization. The following table summarizes the different solutions we prepared:

|                                    |     |      |     |     |     |     |     |      |
|------------------------------------|-----|------|-----|-----|-----|-----|-----|------|
| Lot number                         | 1   | 2    | 3   | 4   | 5   | 6   | 7   | 8    |
| Ratio of monomers<br>(TVE:BPVE)    | 1:1 | 1:9  | 1:9 | 1:9 | 1:9 | 1:9 | 1:1 | 1:1  |
| % Wt. of the solution<br>(Monomes) | 60% | 40%  | 60% | 50% | 50% | 50% | 60% | 60%  |
| Duration of the<br>process (hours) | 3   | 7.75 | 4.5 | 6   | 4.5 | 3   | 3.5 | 2.75 |
| Degree of<br>polymerization        | 47% | 47%  | 45% | 62% | 55% | 41% | 55% | 42%  |

Achieving around 45% degree of pre-polymerization was important in order to apply spin coating successfully.

The material also has to be transparent, however above 50% solution concentrations the material turned white since we exceeded the limit of solubility. We overcame this by heating the material to 70°C under an inert environment before applying spin coating in order to achieve better solubility. After synthesizing the pre-polymer we filtered it in a 0.2µm Teflon filter to clean the solution and remove polymer clusters. We also diluted the material with Mesitylene before spin coating to achieve best viscosity for obtaining the desired thickness of the PFCB layer.

A NMR check after the final curing of the material showed that heating the material to 120°C for 24 hours wasn't sufficient for full polymerization. Furthermore, in case of the 1:1 ratio of monomers the maximum degree of polymerization was 60%, which we attribute to the fact that TVE is a trifunctional molecule ( has 3 double bonds) while the BPVE molecule is a difunctional molecule (has 2 double bonds) as shown in figure 2.6 section 2.3.1.

Figure 4.2a and b presents three different NMR checks of a solution of 1:9 monomers ratio. After a polymerization of 16 hours in 120°C (4.2a) and after 16 hours in 150°C (4.2b) starting from 50% polymerization each. We can conclude that polymerization occurs above 150°C.

Figure 4.2c presents a NMR check of 1:1 monomers ratio after a polymerization of 16 hours in 150°C. We didn't achieve more than 60% degree of polymerization. The maximum degree of polymerization in case of 1:1 ratio solution is 60% even when working in a temperature of 150°C and 89% in the case of 1:9 monomers ratio.

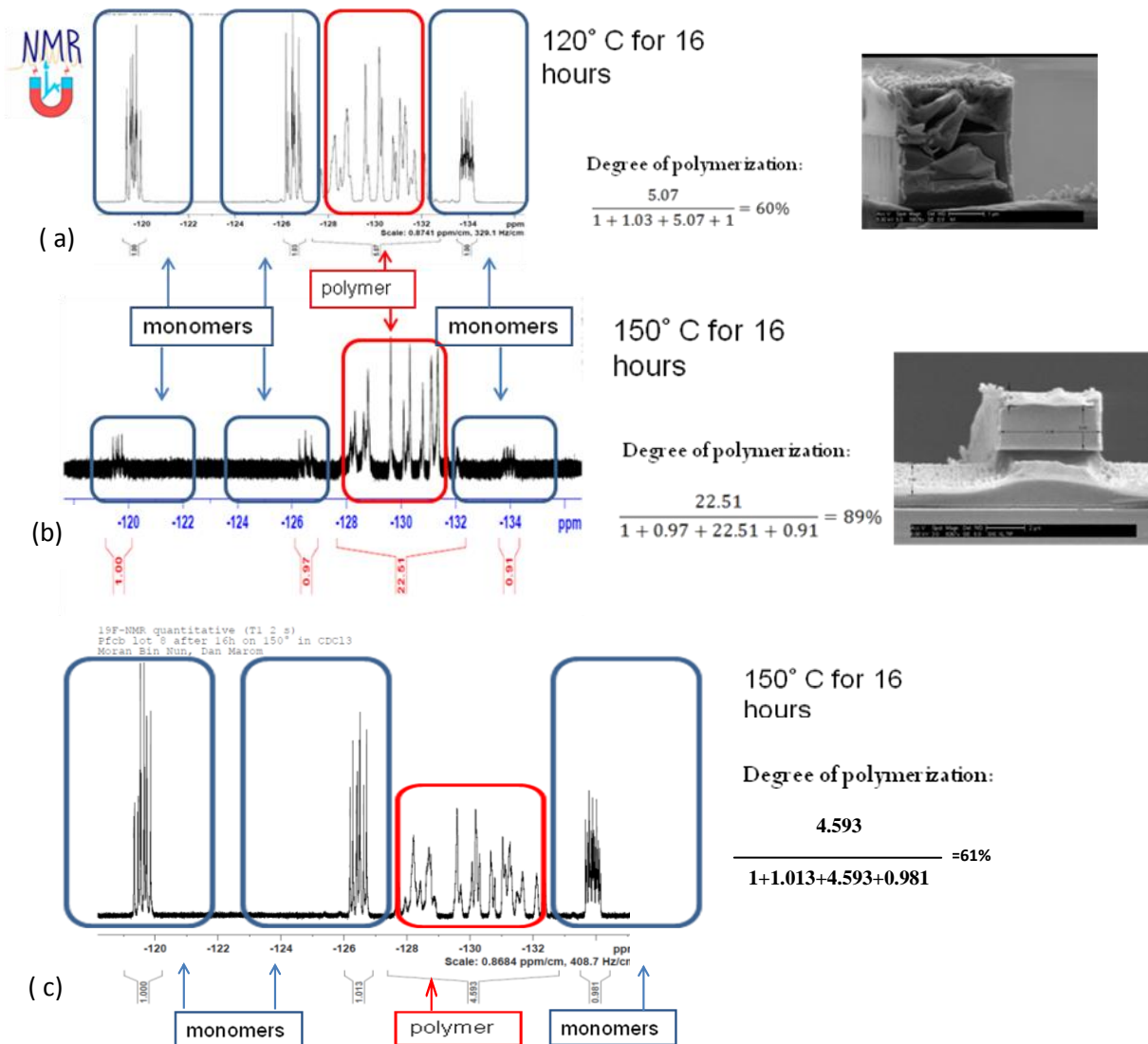


**Figure 4.2:** NMR check in three different cases: a. 1:9 monomers ratio after 16 hours in 120°C. b. 1:9 monomers ratio after 16 hours in 150°C. c. 1:1 monomers ratio after 16 hours in 150°C

We believe that choosing the 1:9 monomers ratio solution will reduce coupling losses of the optical mode since it is easier to dice and polish the device since the PFCB core material is more rigid presenting 89% degree of polymerization. The rigid polymer will also reduce roughness after etching which will reduce the waveguide losses.

### 4.3 Ridge configuration waveguide

#### 4.3.1 Cytop adhesion to silicon

##### Silicon substrate

The device we fabricated was designed in a planar fabrication method. The substrate is a polished silicon wafer. Since Cytop grade A has a poor adhesion to silicon, a surface treatment was needed. We used Silane as a coupling agent. The silicon wafer was agitated for 5 minutes in an Ethanol and Silane solution (0.5% Wt.). Then it was placed on a hot plate set to 180°C for duration of 30 minutes.

#### 4.3.2 Cytop under-clad layer

##### Cytop under-clad

##### Silicon substrate

As was mentioned in section 3.4 a 3.5 $\mu\text{m}$  thick under-clad layer of Cytop was necessary in order to avoid leakage of the optical mode into the silicon substrate. In order to get a uniform layer, spin coating should be done in two steps so the solvent could evaporate better [27]. The spinning condition was also divided into two steps: The first was at 600 rpm for duration of 10 seconds and ramp level 3 in order to homogeneously spread the Cytop on the wafer. The second was at 2000 rpm for duration of 45 seconds and ramp level 3 in order to achieve a 1750 nm thickness layer. We placed the wafer on a hot plate set to 60°C for duration of an hour then we gradually raised it to 95°C for another hour. Finally we raised it to 180°C for 20 minutes for partial curing of the Cytop. The second step was the same only that the final curing of 180°C was set for 3 hours in order to get a fully cured layer. Figure 4.3 presents an optical profilometer image of the Cytop homogenous layer. It can be seen that the maximum vertical deviation is 20nm.

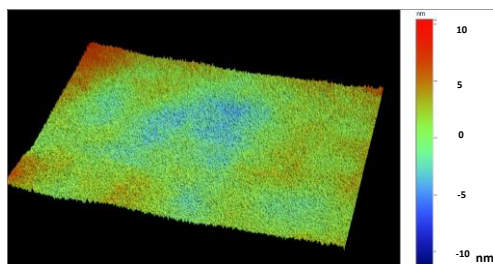
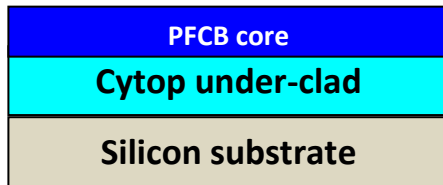


**Figure 4.3:** An optical profilometer image of the Cytop homogenous layer

### 4.3.3 PFCB core layer- adhesion to Cytop



PFCB is a semi fluorinated polymer which is dissolved in Mesitylene solvent. As mentioned in section 4.2 the PFCB is at 45% pre-polymerized state in solution. Hence we can apply spin coating followed by final curing in the oven set to 150°C under an inert environment.

However when we tried to spin coat PFCB directly on the Cytop layer, the Cytop repulsed the PFCB material and we couldn't even spread it on the Cytop layer, before even trying to bond it to the Cytop surface.

The assumption was that there were no sufficient open bonds in the Cytop surface, therefore we applied only partial curing to the Cytop and then tried to spin coat PFCB. After this attempt also failed we tried four different solutions to address this adhesion issue:

- 1) Silane mono layer as adhesion promoter
- 2) 50nm thickness of SiO<sub>2</sub> adhesive layer
- 3) 100 nm thickness PMMA adhesive layer
- 4) PFCB directly on Cytop

#### 4.3.3.1 Silane mono layer

We used Silane as a coupling agent. The Cytop under-clad layer was agitated for 5 minutes in a solution of Ethanol and Silane, 0.5% Wt. Then it was placed on a hot plate set to 100°C for duration of 30 minutes. The reason we set it to 100°C was due to the fact that Cytop glass transition temperature (T<sub>g</sub>) is 108°C [28].

Spin coating in this attempt also failed.

#### 4.3.3.2 50nm thickness of SiO<sub>2</sub>

In previous work, SiO<sub>2</sub> deposition was used with ICP CVD machine set to 40°C stage temperature. However, after raising the PFCB polymerization temperature to 150°C, cracks appeared due to CTE mismatch (figure 4.4). We solved it by raising the deposition temperature to 90°C.

The conditions of the deposition were: 12.9sccm N<sub>2</sub>O, 4sccm SiH<sub>4</sub>, 1000 RF power, 90°C stage temperature for 3 min durations in order to get 50nm layer thickness.

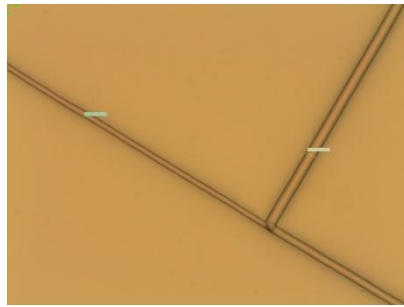


**Figure 4.4:** Cracks in PFCB over 60nm SiO<sub>2</sub> layer deposited in ICP CVD in 40°C

However ICP CVD machine was no longer available for deposition use so we had to use plasma enhanced chemical vapor deposition (PECVD) for SiO<sub>2</sub> deposition instead.

In order to avoid cracks after PFCB curing we had to obey two constraints: First, the temperature of the wafer stage while depositing SiO<sub>2</sub> should be high, but not beyond 108°C due to the limitation of Cytop's T<sub>g</sub>. Second, the SiO<sub>2</sub> layer should be as much physically compressive as possible. This is achieved by reducing the flow rates of the gases participating the process (SiH<sub>4</sub>:N<sub>2</sub>O) while keeping a ratio of 1:25 between them to maintain the SiO<sub>2</sub> chemical structure.

Finally the conditions of the SiO<sub>2</sub> deposition were:

First step of 20sccm N<sub>2</sub>, 1500mtorr chamber pressure, 100°C stage temperature for duration of 5 minute in order to make sure the wafer carrier achieves the 100°C temperature. Second step of 100°C stage temperature for 5 min duration without gas flow and pressure. Last step of 100°C stage temperature for duration of 3 minute with 400 mtorr chamber pressure and 50 sccm N<sub>2</sub>O, 2 sccm SiH<sub>4</sub> and 300sccm Ar flow rates. The last step was the deposition step. Ar isn't reactive and was added to this step only to enhance the plasma while still keeping the low deposition rate. A SiO<sub>2</sub> deposition rate of 20nm/min was obtained.

After spin coating of the PFCB the spreading succeeded although after curing in an inert environment in a temperature of 150°C which is necessary for the polymerization of the PFCB, some deformations appeared in the PFCB material (figure 4.5). Apparently 100°C wasn't sufficient to overcome CTE mismatch. After raising the temperature to 150°C no cracks appeared, however we abandoned this

solution since this temperature was above Cytop Tg which means that SiO<sub>2</sub> particles probably diffused the Cytop layer.

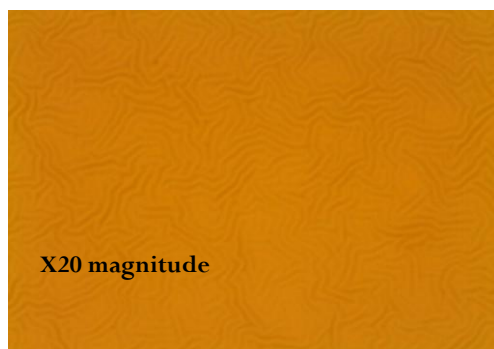


**Figure 4.5:** deformation in PFCB polymer layer

#### **4.3.3.3 100nm thickness PMMA**

In order to achieve good adhesion to the Cytop, a layer of at least 100 nm PMMA is necessary. First we applied plasma ashing to the Cytop surface in the following conditions: 40% power, 0.2 Psi O<sub>2</sub> for a duration of 0.5 minute. This step enabled PMMA to adhere Cytop.

We applied spin coating of PMMA in two steps. The conditions of the first step: 600 RPM for duration of 2 seconds in order to spread it homogenously on the Cytop. The conditions of the second step: 1500 RPM for duration of 45 seconds in order to get a layer of 100nm thickness which enabled the next PFCB layer to adhere. It is important to mention that when we used a PMMA layer below 100 nm thickness, the next PFCB layer couldn't adhere.

We finally applied spin coating of PFCB in the conditions: 600 RPM for 7 seconds followed by 1500 RPM for 45 seconds. After 6 hours curing in the oven set to 150°C under an inert environment, there were no cracks observed.

However using an external material in order to couple Cytop and PFCB wasn't an elegant solution since it may cause some other problems such as losses and stresses which lead to birefringes.

#### **4.3.3.4 PFCB directly on Cytop**

We tried to couple PFCB and Cytop directly. We added Chloroform solvent to the solution of PFCB. Chloroform is a polar solvent since the electronegativity of Chlorine and Hydrogen is 3 and 2.1, respectively, whereas the structure of Mesitylene is A-polar since the three polar CH<sub>3</sub> bonds balance each other (figure 4.6). Cytop has also polar molecules since it is COOH terminated and therefore can attract the PFCB

solution with the chloroform better than with the Mesitylene alone, however we still use Mesitylene along with chloroform since its boiling temperature is high (163°C) in comparison to Chloroform (61.2°C) which is essential for the rest of the polymerization process which occurs in 150°C.

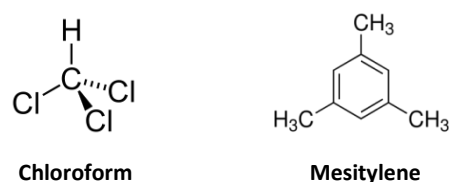


**Figure 4.6 :** Chloroform and Mesitylene molecules

Prior to PFCB spin coating we applied plasma ashing to the Cytop surface in the following conditions: 40% power , 0.3 mbar O<sub>2</sub> for a duration of 0.5 minute. We poured PFCB and spread it manually by slightly agitating the wafer. Finally we applied spin coating in the conditions: 600 rpm for 2 seconds followed by 1500 rpm for 45 seconds.

As we expected, the PFCB didn't moved away as it did without adding Chloroform to the PFCB solution. However, after we applied curing in the oven set to 150°C under an inert environment, islands of PFCB observed (figure 4.7). Probably the capillary forces in which the liquid move along the surface due to the attraction between the liquid and the solid molecules were stronger than the weak adhesion between PFCB solution and Cytop.

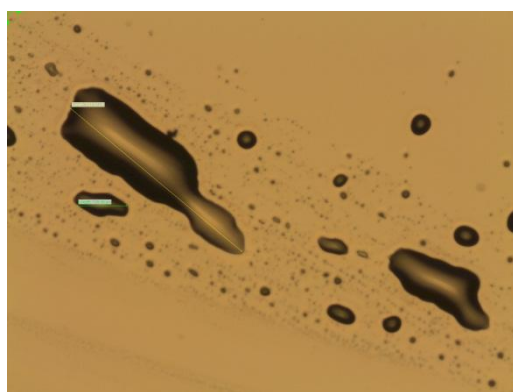


**Figure 4.7:** Islands of PFCB

Therefore before applying curing we applied plasma ashing: 40% power , 0.3 mbar Ar for a duration of 0.2 minute. This step evaporated some of the solvent and made the material more viscous preventing it from moving. We used Ar plasma rather than O<sub>2</sub> plasma to avoid oxidation of PFCB.

After we applied curing in the oven set to 150°C under an inert environment, there were no cracks or islands observed and we got a good adhesion.

#### 4.3.4 Etching Selectivity

Prior to lithography step we had to decide whether the 500nm AZ1505 photoresist (PR) layer was sufficient for etching 1500nm PFCB ridges. In order to do so we covered half of the AZ1505 PR layer with a mechanical mask and applied reactive ion etching (RIE) using ICP-RIE Oxford Instruments Plasmalab System 100 plasma etcher machine. We carried on *polymer etch* recipe with the following conditions: 2 mtorr chamber pressure and 10 sccm O<sub>2</sub> at 20°C for duration of 10 sec. We got a valley of 94nm in the AZ1505 PR (figure 4.8a). That means that the etch rate of the PR using *polymer etch* was 564nm/min. However when we applied the same recipe on PFCB for 1 min duration, we got a valley of 650nm which means that the etch rate of the PFCB using *polymer etch* was 650nm/min (figure 4.8b). We therefore concluded that the selectivity of PFCB: AZ1505 PR is 1.2:1. That means that in order to etch 1500nm PFCB ridges a 1250nm PR layer is required. This is of course not a solution since such a thick PR layer would harm the resolution.

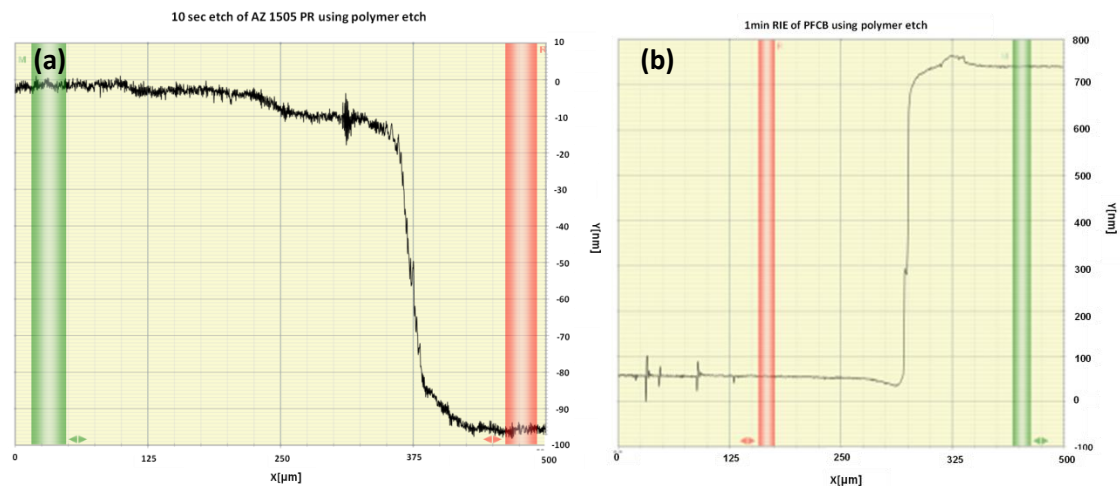
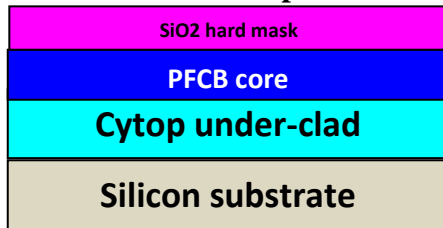


**Figure 4.8:** a. 10 sec RIE of AZ1505 using polymer etch: 94nm b. 1min RIE of PFCB using polymer etch: 650nm

The reason for the low selectivity is due to the fact that the PR is also an organic polymer and therefore can be easily etched by O<sub>2</sub> plasma therefore it is impossible to achieve the desired aspect ratio with the use of a PR mask only.

We had to use another material which will survive the 1500nm PFCB etch. This material should have a different sensitivity for the etching chemistry (high selectivity). This element is referred as a hard mask.

#### 4.3.5 Deposition of 50nm SiO<sub>2</sub> layer as hard mask



WE chose as a hard mask material silicon dioxide (SiO<sub>2</sub>) deposited in low temperature of 100<sup>0</sup>C with PECVD in the conditions mentioned in section 4.3.3.2. In order to determine the thickness of the SiO<sub>2</sub> layer we applied 2 min *polymer etch* on a half covered SiO<sub>2</sub> layer. We got a valley of 26nm (figure 4.9) .That means that the etch rate is 13nm/min therefore the selectivity of SiO<sub>2</sub>:PFCB is 1:41.

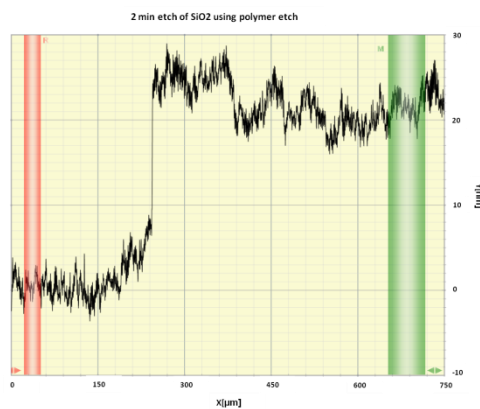


**Figure 4.9:** 1min RIE of SiO<sub>2</sub> using *polymer etch*

We concluded that a 50nm thickness of SiO<sub>2</sub> was more than enough for 1500nm PFCB ridges. (Less than 50nm presented adhesion problems).

In order to determine whether the 500nm PR were sufficient for the 50nm SiO<sub>2</sub> we applied *SiO<sub>2</sub> etch* on a half covered AZ1505 PR in the following conditions:15 mtorr chamber pressure and 50 sccm CHF<sub>3</sub> and 50 sccm Ar flow rates at 20°C stage temperature for duration of 1 minute each. 39nm valley was achieved (figure 4.10). The selectivity of (SiO<sub>2</sub>: AZ1505 PR) is therefore 1:2.3. 500nm PR was more than sufficient for 100nm SiO<sub>2</sub>.

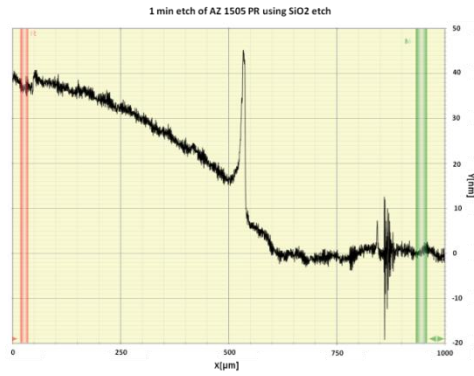
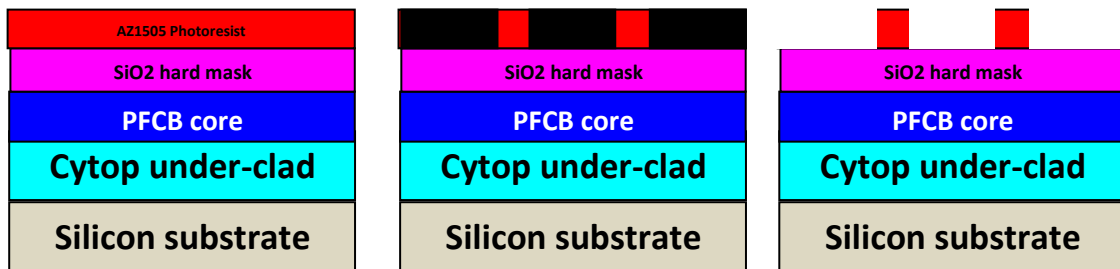


**Figure 4.10:** 1 min RIE of AZ1505 using *SiO<sub>2</sub> etch*: 39nm

It is important to mention that in our previous fabrication we deposited 200nm SiO<sub>2</sub> layer thickness as the hard mask using ICP CVD in 40<sup>0</sup>C with faster flow rate as mentioned in section 4.3.3.2, however cracks appeared in the lithography step due to CTE mismatch. To avoid the cracks the hard mask was deposited on the Cytop upper clad.

Changing the SiO<sub>2</sub> deposition conditions and depositing a thinner layer (50nm) allowed us to deposit the hard mask directly on PFCB without forming cracks which made the process easier and more controllable.

#### 4.3.6 Lithography and development



To achieve a resolution of 1 $\mu$ m, AZ1505 photoresist was used. Prior to spin coating of the photoresist the wafer was placed in a hot plate set to 100<sup>0</sup> for duration of 5 minute in order to remove humidity. This step was necessary to help the next PR polymer adhesion to succeed. The conditions of the photoresist spin coating: 600 rpm for duration of 3 second at ramp level 3 in order to spread the photoresist homogenously on the wafer, followed by 4000 rpm for duration of 30 seconds and ramp level 3 to achieve a 0.5 $\mu$ m photoresist layer. Afterward the photoresist covered wafer was placed in a hot plate set to 100<sup>0</sup> for duration of 10 minutes (prebake).

Finally the wafer was placed in the lithography SUSS mask aligner. The lithography conditions: vacuum contact, exposure type and 1 second UV exposure time. In order to make a ridge configuration a positive mask was used since the AZ1505 PR is a positive resist.

After the exposure step was complete PR development was necessary. The wafer was placed in AZ 726 developer and was agitated for duration of 15 seconds. It was then washed in water and dried in Nitrogen.

Figure 4.11 presents a top view of the ridges after development.

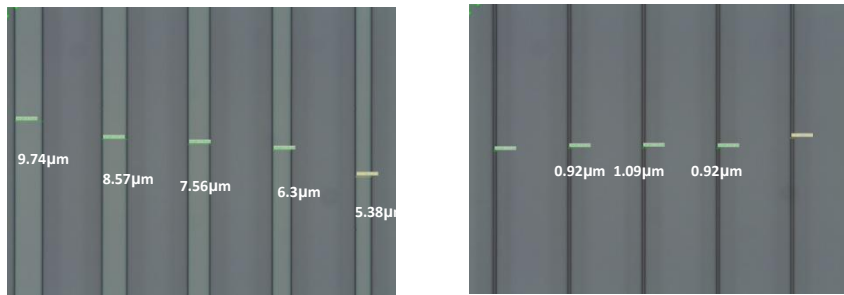
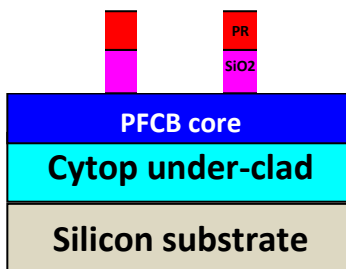


**Figure 4.11:** Top view of different width ridges after development.

a. 10 μm, 9 μm, 8 μm, 7 μm, 6 μm planned waveguides width. b. 1.5 μm planned waveguides width.

As can be seen there is a deviation of approximately 0.4 μm-0.6 μm in the waveguide width after lithography and development.

#### 4.3.7 RIE



We applied reactive ion etching (RIE) using ICP-RIE Oxford Instruments Plasmalab System 100 plasma etcher machine.

In order to etch 50 nm SiO<sub>2</sub> we used *SiO<sub>2</sub> etch* for a duration of 1 min. The etch rate of a sharp edge was 90 nm/min (figure 4.12) however for smaller features (1 μm order of magnitude) the rate is even slower. Therefore, 1 min duration was taken in order to make sure no SiO<sub>2</sub> was left, otherwise the next PFCB etch wouldn't succeed.

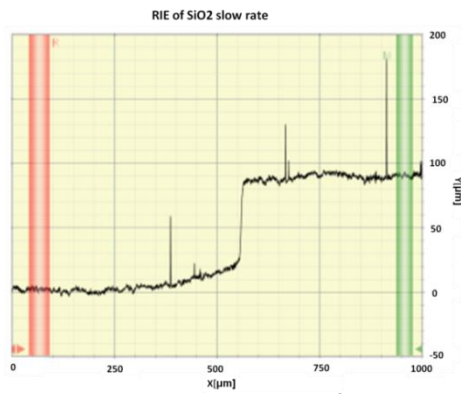
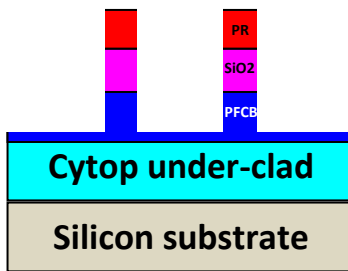


Figure 4.12: 1min  $SiO_2$  etch of  $SiO_2$ : 90nm



In the following step etching 1500 nm of PFCB is required.

In order to determine the *polymer etch* duration we first applied *SiO<sub>2</sub> etch* on a half covered PFCB layer for 1min duration. 39nm valley was achieved (figure 4.10). We used *polymer etch* recipe for 2 minutes duration since the PFCB etch rate was 650nm/min (figure 4.8b).

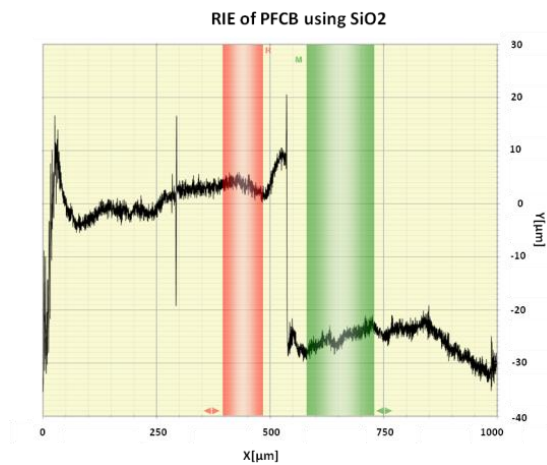
The reason we etched only 1300nm PFCB by time is to get a ridge waveguide which is better adhered to Cytop than a squared one. However after applying this step the wafer turned white, which indicated that there wasn't enough heat removal during etching. Therefore, we divided the PFCB etch into three periods of time, 40 sec each, to allow for heat removal. We also reduced wafer clamp temperature to 5°C. Reducing the temperature also improved the etching performance in a way which made the side walls straighter. Under those conditions the wafer didn't turn white. The PR should be almost completely removed and even if there were some remainders, they would disappear after removing the  $SiO_2$  hard mask.

Another etching technique we used was  $O_2:SF_6$  etch in 1:3 ratio as reported in Nazli thesis [29], however using  $SF_6$  also etched the  $SiO_2$  hard mask (1:2.6 selectivity of PFCB: $SiO_2$ ) which meant that in order to etch 1500nm PFCB we had to deposit 580nm  $SiO_2$ . To avoid stresses we decide to use 120nm Al as hard mask. It is important to mention that when we deposited below 120nm of Al, the layer didn't survive the lithography process and was ruined when we applied humidity removal and prebake.

We finally decided to abandon this solution since the final removal of the Al destroyed the PFCB core layer and to use the previous O<sub>2</sub> etch using a temperature of 5°C.

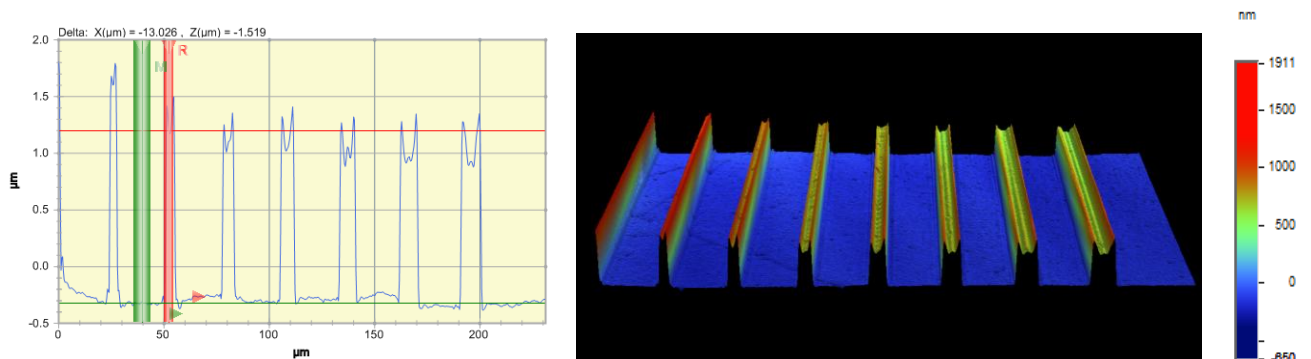


Finally we removed the SiO<sub>2</sub> hard mask using *SiO<sub>2</sub> etch* recipe as we did before. It is important to mention that removing the SiO<sub>2</sub> etched only 30nm PFCB layer as can be seen in figure 4.13 where SiO<sub>2</sub> etch was applied on a half covered PFCB layer for duration of 1 min.



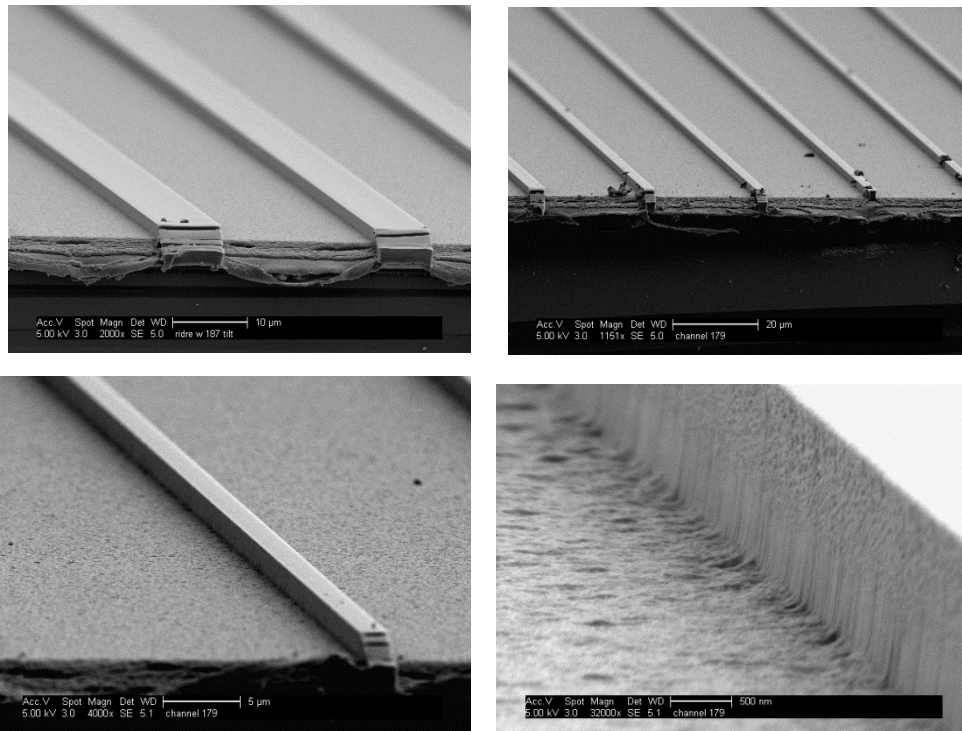
**Figure 4.13:** 1 min etch of PFCB using *SiO<sub>2</sub> etch*: 30nm

Figure 4.14 shows an optical profilometer image of a 1500nm height of the fabricated ridge. The width of the waveguide presented are 10μm, 9μm, 8μm, 7μm, 6μm, 5μm, 4μm and 3μm. The top side pattern is due to edge effects of the optical profilometer.



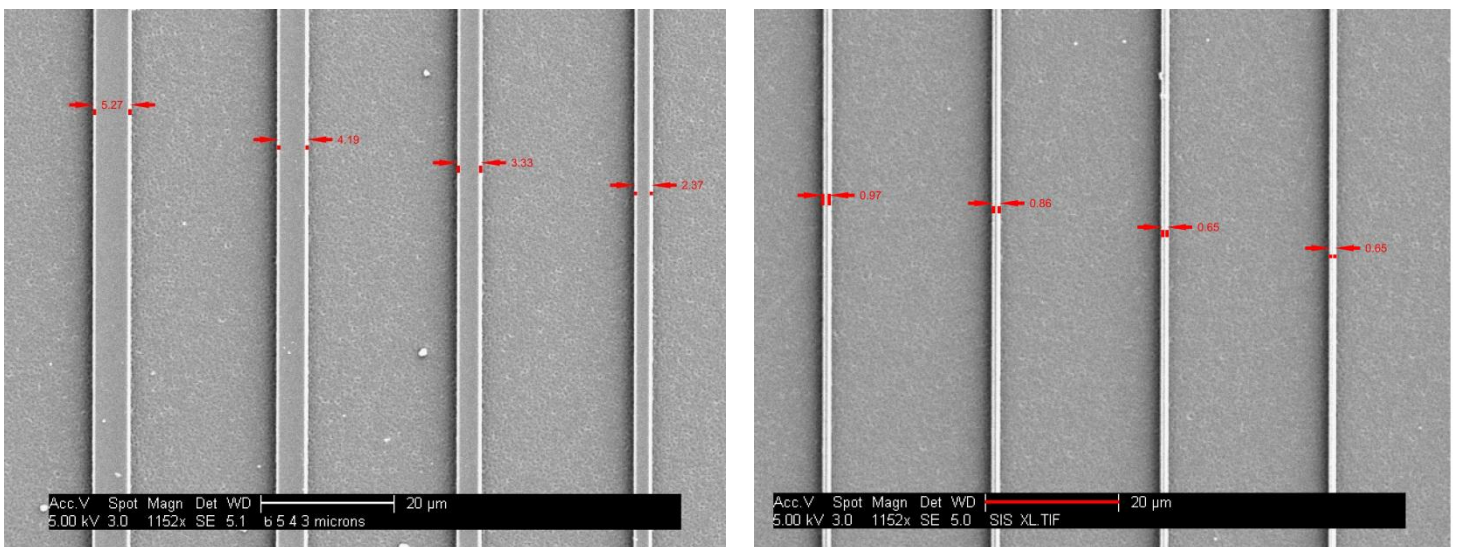
**Figure 4.14 :** Optical profilometer images of ridge configuration at 10μm, 9μm, 8μm, 7μm, 6μm, 5μm, 4μm and 3μm waveguide width.

Figure 4.15 shows SEM images of PFCB ridges at height of 1.5 $\mu$ m with different widths.



**Figure 4.15:** SEM images of different width PFCB ridges at 1.5  $\mu$ m height

In order to determine the total deviation from the width of waveguides we planned, we took a top view of the waveguides using SEM (figure 4.16).

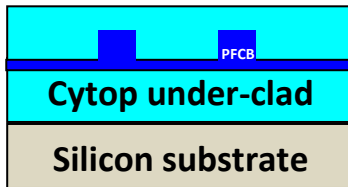


**Figure 4.16:** SEM image of different width PFCB ridges at 1.5  $\mu$ m height

- a. 6 $\mu$ m, 5 $\mu$ m, 4 $\mu$ m and 3 $\mu$ m planned waveguide width
- b. 1.5 $\mu$ m, 1.5 $\mu$ m, 1.4 $\mu$ m and 1.2 $\mu$ m planned waveguide width

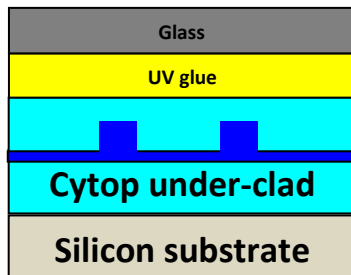
We can conclude that there is a deviation of approximately  $0.5\mu\text{m}$  to  $0.8\mu\text{m}$  in the width of the waveguides. As expected there is narrowing of the lines after applying RIE. Therefore in order to get  $1.5\mu\text{m}$  width waveguide, we need to plan widths of  $2\mu\text{m}$ ,  $2.1\mu\text{m}$ ,  $2.2\mu\text{m}$ ,  $2.3\mu\text{m}$  and  $2.4\mu\text{m}$ .

#### 4.3.8 Cytop over clad



We applied plasma ashing to the PFCB surface in the following conditions: 40% power, 0.3 mbar  $\text{O}_2$  for a duration of 0.5 minute. This step enables Cytop to adhere PFCB. We applied spin coating of Cytop in the conditions: 600 rpm for a duration of 10 seconds followed by 1000 rpm for 45 seconds. We cured it in the oven set to  $150^\circ\text{C}$  for duration of 4 hours. We repeated this procedure in order to get a  $3.5\mu\text{m}$  homogenous layer. No cracks were observed.

#### 4.3.9 Glass cover



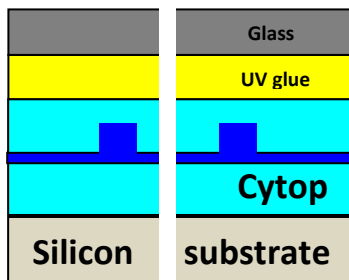
In order to access the waveguides we needed to dice the wafer and follow with polishing of the device edges. To withstand both the dicing and polishing, it was essential to cover the wafer with a glass substrate ( $200\text{nm}$ ).

We applied a short  $\text{O}_2$  plasma ashing surface treatment for 30 seconds. The glass was cleaned in Acetone, Isopropanol and water and was dried in Nitrogen. Afterwards it was placed on the hot plate set to  $100^\circ\text{C}$  to remove humidity.

We poured the UV glue (Norland optical adhesive 61) on the over clad Cytop layer and placed the clean glass on it.

In order to achieve as thin layer as possible the wafer and the cover glass were squeezed by hand and was put in a mask-aligner set to 40 seconds UV exposure time.

#### 4.3.10 Dicing and polishing



Dicing is an important step that exposes the input and output waveguide facets for in and out coupling of light once waveguide devices are fabricated on the substrate. The dicing was done using with a diamond saw speed of 1.5mm/sec. Polishing the edges was done in seven steps of polishing diamond films from 15 $\mu$ m to 0.1 $\mu$ m grid.

Figure 4.17 present a edge facet of the polished square WG.

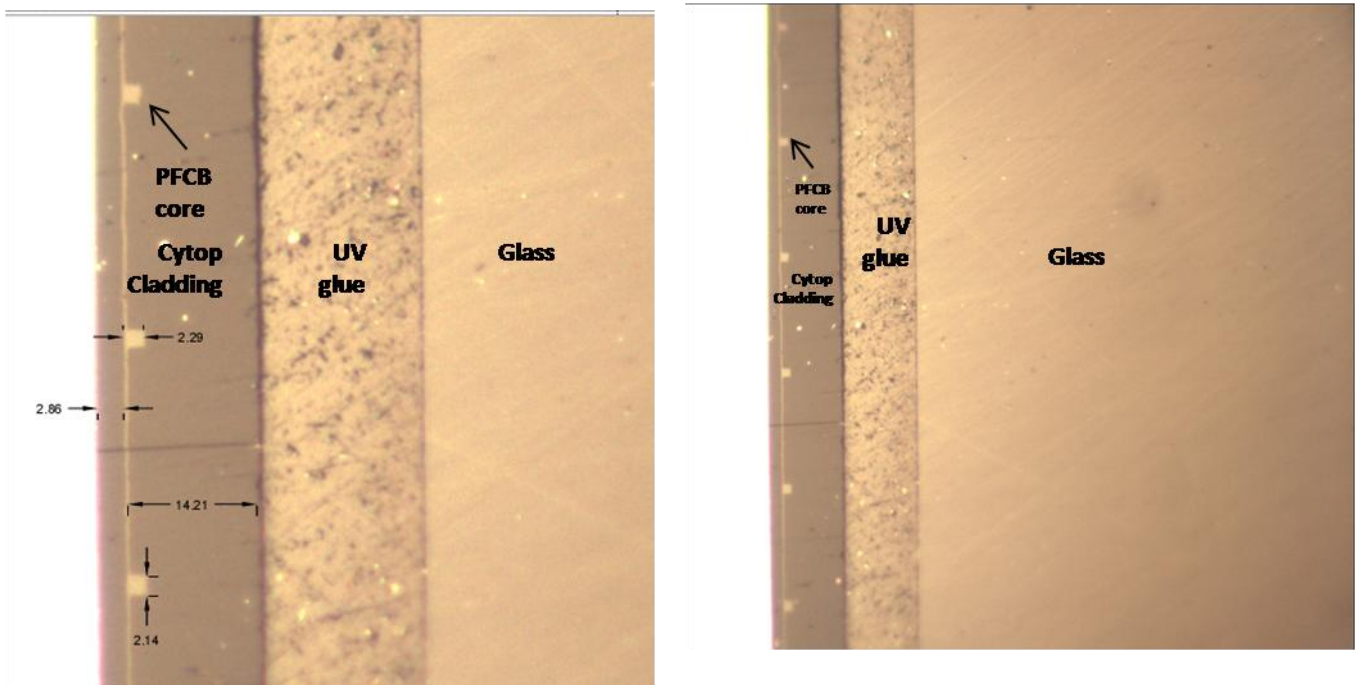


**Figure 4.17:** a cross section of the polished square WG fabricated in the ridge method.

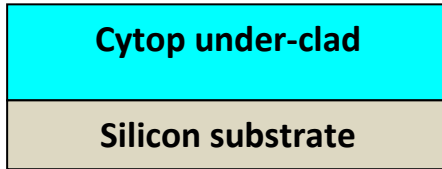
#### 4.4 Trench configuration waveguide

Since our final objective is to design nonlinear waveguides which are achieved by doping the PFCB core with semiconductor nanocrystals, we must design a process that will be compatible with the semiconductor nanocrystals material.

Problems may occur during the RIE process since the recipe of the PFCB etch won't necessary be suitable to the nanocrystals material. Furthermore we are limited in the materials allowed inside the RIE machine, since some of the NCs may cause contamination to the machine.

Here we tried to plan fabrication configuration that achieve nonlinear WG without applying RIE to the PFCB core.

#### 4.4.1 5 $\mu$ m Cytop layer



We carried out a surface treatment using Silane to the Silicon surface as we did in the ridge configuration in section 4.3.1. In order to design a trench configuration, a 5 $\mu$ m thickness of Cytop layer is needed. The process was the same as in the ridge configuration in section 4.3.2 only that we repeated it for three times in order to get a thicker layer.

#### 4.4.2 Etching selectivity

As mentioned in section 4.3.4 prior to lithography we had to decide whether the PR layer was sufficient for etching 1500nm depth trenches. Here we present two methods. The first is dealing with the same positive AZ1505 PR that we used in the ridge configuration. We already examined the etch rate of this PR (564nm/min). The trenches are going to be etched in the Cytop therefore in order to determine the selectivity, the Cytop etch rate is required. A half covered Cytop layer was etched using *polymer etch* for 1 min. 1500nm valley was achieved (figure 4.18 ).We concluded that the selectivity is therefore 1:2.7 (PR: Cytop) which means that in order to etch 1500nm trenches in the Cytop,555nm PR is required. It is important to note that this selectivity was achieved for large features however for smaller features (few microns) the selectivity is also smaller therefore 500nm PR will not be sufficient for 1500nm trenches in the Cytop.

We decided to use SiO<sub>2</sub> as adhesive layer and also as hard-mask.

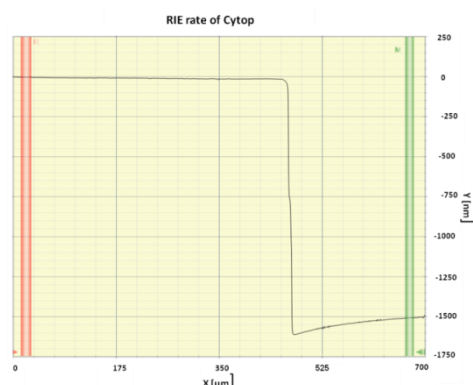


**Figure 4.18:** 1 min etch of Cytop using *polymer etch*: 30nm

Using AZ1505 which is a positive PR required using a negative mask in order to achieve trenches rather than ridges.

Another PR we examined was Ma-N PR which is a negative PR. Using a negative PR allowed us working with the positive mask we used for the ridge configuration. In order to determine the selectivity of Ma-N PR:Cytop we applied 10 sec etch of *polymer etch* on a half covered Ma-N layer. 55nm valley was achieved (figure 4.19) which means that the etch rate of Ma-N PR is 330nm/min. The selectivity of Ma-N PR:Cytop is therefore 1:4.6. In order to etch 1500nm trenches in the Cytop 330nm PR is required. Here also the selectivity was achieved for larger features however for smaller features (few microns) the selectivity is also smaller. However as opposed to the former technique we can use a thicker layer of PR. We started with 50nm SiO<sub>2</sub> layer as a hard mask for both PR methods.

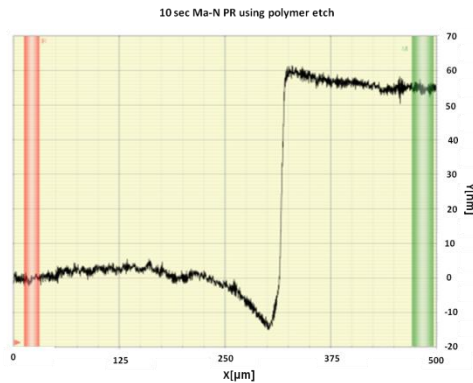
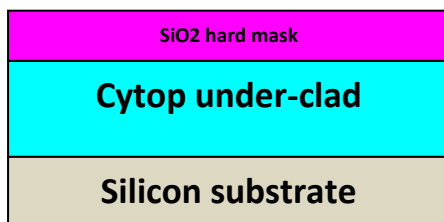


Figure 4.19: 10 sec etch of Ma-N PR using *polymer etch*: 55nm

#### 4.4.3 50nm SiO<sub>2</sub> hard-mask

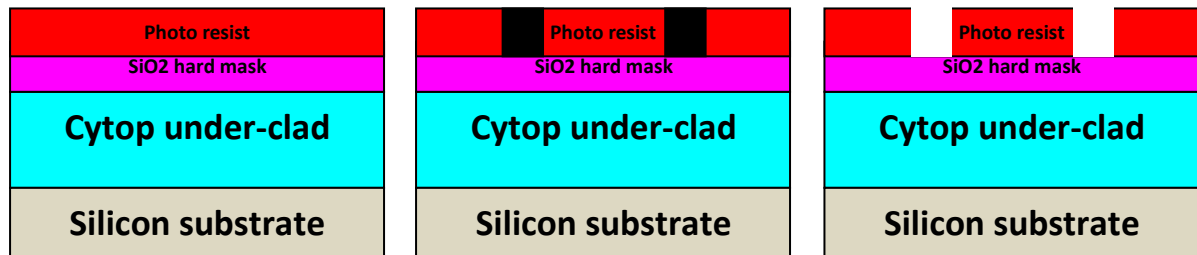


We chose SiO<sub>2</sub> as a hard mask. In order to determine the required width of the SiO<sub>2</sub> layer we used the information in section 5.3.5 where the SiO<sub>2</sub> etch rate using polymer etch was 13nm/min.

The selectivity is therefore: 1:115 (SiO<sub>2</sub>:Cytop). Therefore 50nm thickness of SiO<sub>2</sub> were more than sufficient for etching 1500nm trenches in the Cytop. 500nm AZ1505 PR was also more than sufficient for 50nm SiO<sub>2</sub> (see selectivity of AZ1505 PR: SiO<sub>2</sub> in section 4.3.5).

At first we deposited SiO<sub>2</sub> in the following conditions: low temperature of 100°C at a rate of 60nm/min for duration of 50 sec with 1000 mtorr chamber pressure and 161.5 sccm N<sub>2</sub>O and 8.5 sccm SiH<sub>4</sub>. Using this recipe there were cracks observed . The solution was to reduce the flow rate of the gases which participated the process. Therefore the final recipe was: low temperature of 100<sup>0</sup>C at a rate of 20nm/min for duration of 3 minute with 400 mtorr chamber pressure and 50 sccm N<sub>2</sub>O and 2 sccm SiH<sub>4</sub>.

#### 4.4.4 Lithography and development



In order to etch 50nm SiO<sub>2</sub> layer, 500nm PR thickness were more than enough. We placed the wafer on a hot plate set to 100<sup>0</sup>C for duration of 5 minutes in order to remove humidity. We applied spin coating of PR in the following conditions: 600 rpm for duration of 3 min to spread the material followed by 4000 rpm for duration of 45 minutes to get the desired 500nm thickness. The wafer was placed on a hot plate set to 100<sup>0</sup>C for prebake.

We inserted the wafer to the mask aligner and exposed UV radiation for duration of 0.9 seconds with a vacuum type exposure. The wafer was then agitated for 15 seconds in AZ 726 developer, washed in water and dried in Nitrogen. In order to make a trench configuration a negative mask was used since the AZ1505 PR is a positive resist.

Another way was to use the positive mask we had and using a negative photoresist.

In the second method where we used Ma-N negative PR, the wafer was placed on the hot plate set to 100<sup>0</sup>C for 5min to remove humidity. Few monolayers of HDMS adhesion promoter were added in the spinner at 3000rpm for 30sec followed by 500nm Ma-N PR achieved by 3000rpm for 30sec. The wafer was placed on a hot plate set to 100<sup>0</sup>C for one min (prebake). We applied lithography in contact type for 9sec exposure. The wafer was placed on a hot plate set to 100<sup>0</sup>C for one min (postbake) which was necessary for negative PRs. We applied development using Ma-D developer for 55sec and finally placed it on the hot plate set to 100<sup>0</sup>C for another

1min (hardbake). Figure 4.20 Present a top view of the trenches after 55sec development

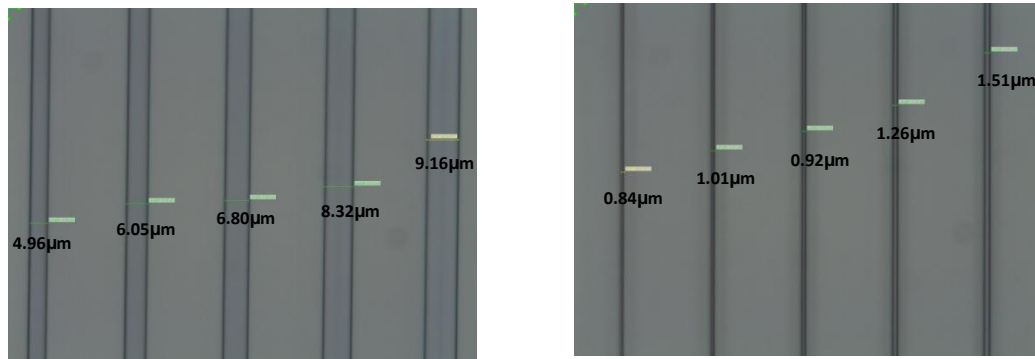
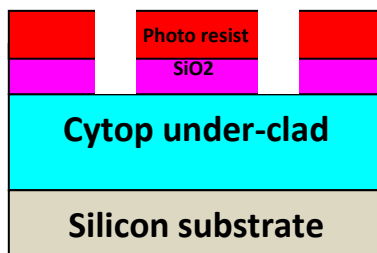


**Figure 4.20** Top view of different width trenches after development.

a. 10µm,9µm,8µm,7µm,6µm planned waveguides width. b. 2.4µm, 2.2µm, 2µm, 1.8µm and 1.6µm planned waveguides width.

As can be seen there is a width deviation of 0.8µm-1.2µm due to lithography and development process. It is important to note that we can do further optimization, either by shortening the exposure time or by extending the development time.

#### 4.4.5 RIE



Next, we applied reactive ion etching (RIE) using ICP-RIE Oxford Instruments Plasmalab System 100 plasma etcher machine. In order to etch 50 nm SiO<sub>2</sub> we used 1 min *SiO<sub>2</sub> etch* (90nm/min etch rate) in order to make sure that no SiO<sub>2</sub> was left. In the following step we wished to etch 1500 nm trenches depth in Cytop. In order to determine the depth of the trenches in the Cytop we applied 1 min *SiO<sub>2</sub> etch* on a half covered Cytop layer. 680nm valley was achieved (figure 4.21). That meant that the final removal of the 50nm SiO<sub>2</sub> would etch another 680nm Cytop, however etching in a trench had a lower rate (150nm/min). Therefore instead of etching 1500nm of Cytop trenches we etched only 1200nm. We used *polymer etch* for 48 sec.

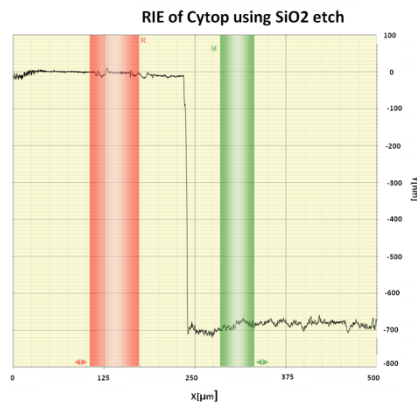
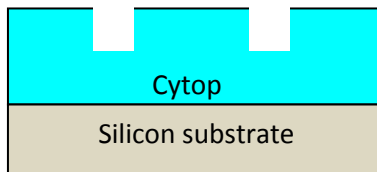


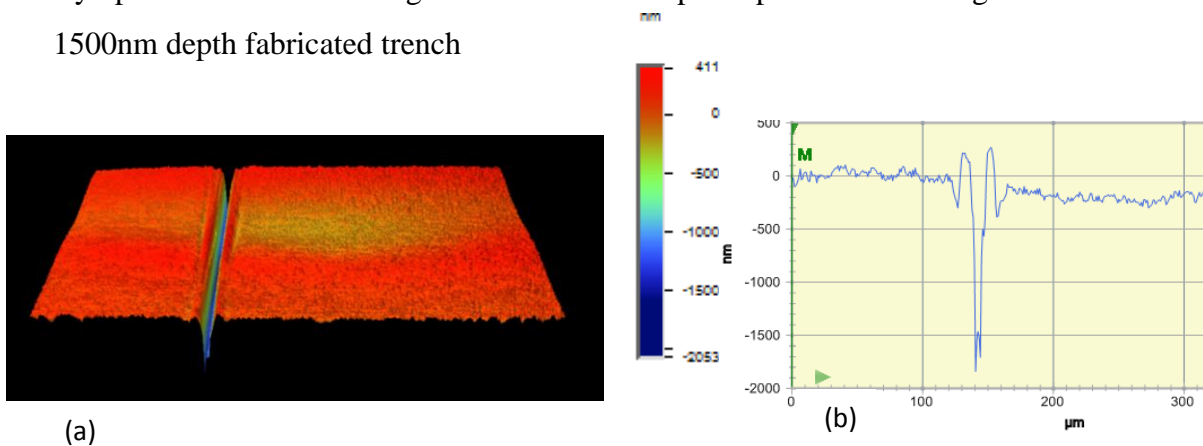
**Figure 4.21** : RIE of Cytop using SiO<sub>2</sub> etch: 680nm/min

In this level we were sure that the photoresist was removed almost completely. And even if there were some remainders, they would disappear after removing the SiO<sub>2</sub> hard mask.



Finally we removed the SiO<sub>2</sub> hard mask using *SiO<sub>2</sub> etch* for 1 min duration.

By using trench configuration the only polymer which went through etching was Cytop rather than PFCB. Figure 4.22 shows an optical profilometer image of a 1500nm depth fabricated trench



(a)

(b)

**Figure 4.22** : a. A three dimensions optical profilometer image of a 1500nm deep trench

b. A cross section of the trench

Figure 4.23 presents SEM images of the trench configuration of different width trenches.

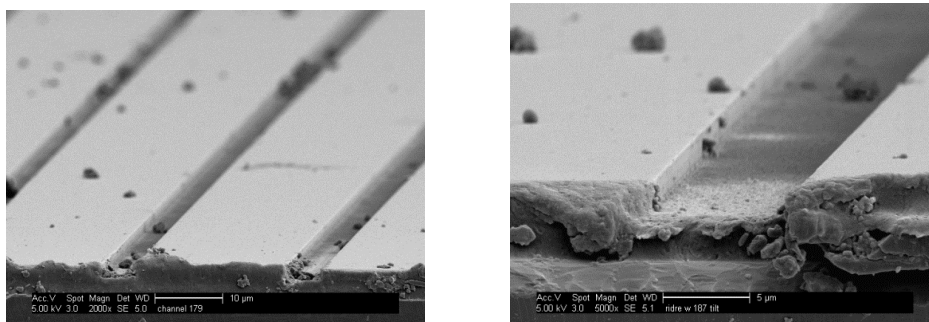


**Figure 4.23:** SEM images of trenches 1.5μm depth. Scattered particles are from cleavage step

Before filling the trenches with PFCB it is essential to clean it in order to remove the particles observed.

In order to determine the total deviation from the width of waveguides we planned, we took a top view of the waveguides using SEM (figure 4.24).

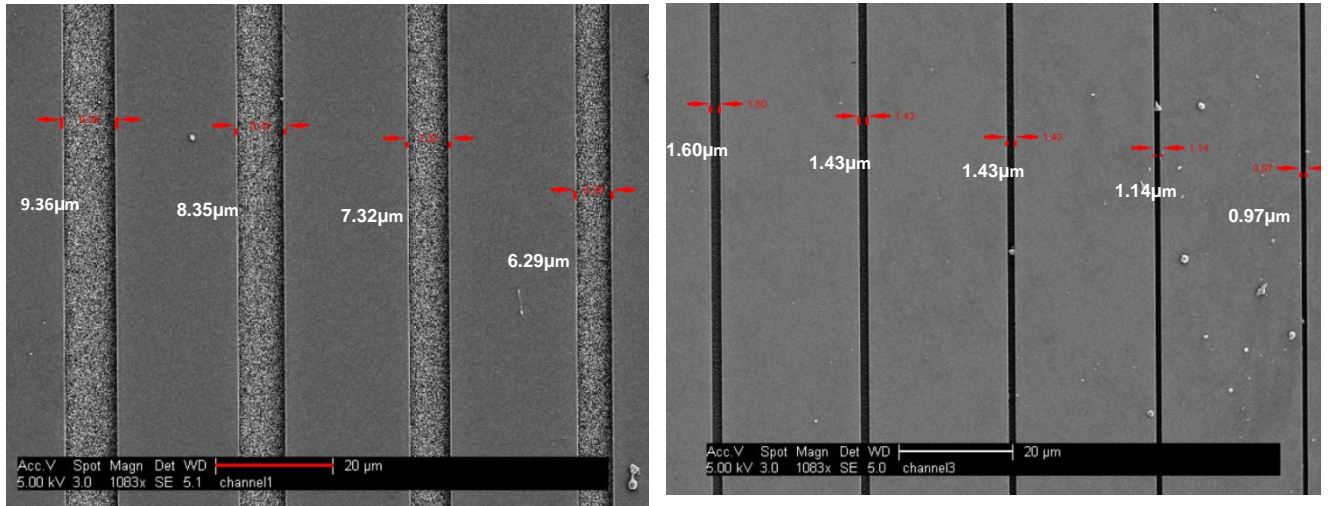


**Figure 4.24** : SEM image of different width PFCB ridges at 1.7  $\mu\text{m}$  height

- 10 $\mu\text{m}$ , 9 $\mu\text{m}$ , 8 $\mu\text{m}$  and 7 $\mu\text{m}$  planned waveguide width
- 2.4 $\mu\text{m}$ , 2.2 $\mu\text{m}$ , 2 $\mu\text{m}$ , 1.8 $\mu\text{m}$  and 1.6 $\mu\text{m}$  planned waveguide width

We can conclude that there is a deviation of approximately 0.6 $\mu\text{m}$  to 0.8 $\mu\text{m}$  in the width of the waveguides. As expected the RIE process enlarged the trenches after lithography process (the deviation from the real value is smaller). Therefore in order to get 1.5 $\mu\text{m}$  width waveguide, we need to plan widths of 2.1 $\mu\text{m}$ , 2.2 $\mu\text{m}$  and 2.3 $\mu\text{m}$ .

However we can carry on with the optimization of the lithography condition in order to enlarge the lines.

#### 4.4.6 Further optimization

As was mentioned in 4.4.2 the selectivity of Ma-N PR: Cytop was 1:4.6 which means that 330nm of PR could be sufficient for 1500nm trenches of Cytop.

By using only PR without SiO<sub>2</sub> as hard mask we simplify the fabrication process and also avoid stress due to the SiO<sub>2</sub> layer.

We first applied 0.5 min O<sub>2</sub> plasma ashing with 40% power on the 5 $\mu\text{m}$  Cytop layer. We used a 500nm Ma-N PR thickness directly on the Cytop layer in the same conditions mentioned in section 4.4.2 only without HDMS adhesion promoter (since it was an adhesion promoter for SiO<sub>2</sub>/metals –PR interfaces). The lithography process was the same as mentioned in section 4.4.4. We applied RIE of polymer etch for 80

seconds duration. However only 1100nm trenches were achieved (figure 4.25a). In order to determine whether the reason is lack of PR mask or lack of etch duration we added another 20 sec of *polymer etch*. The depth of the trenches remained the same (figure 4.25b ) which meant that no PR was left. Therefore we concluded that 500nm PR wasn't sufficient for 1500nm trenches. Also that the selectivity of Ma-N PR:Cytop for few microns features is 1:2

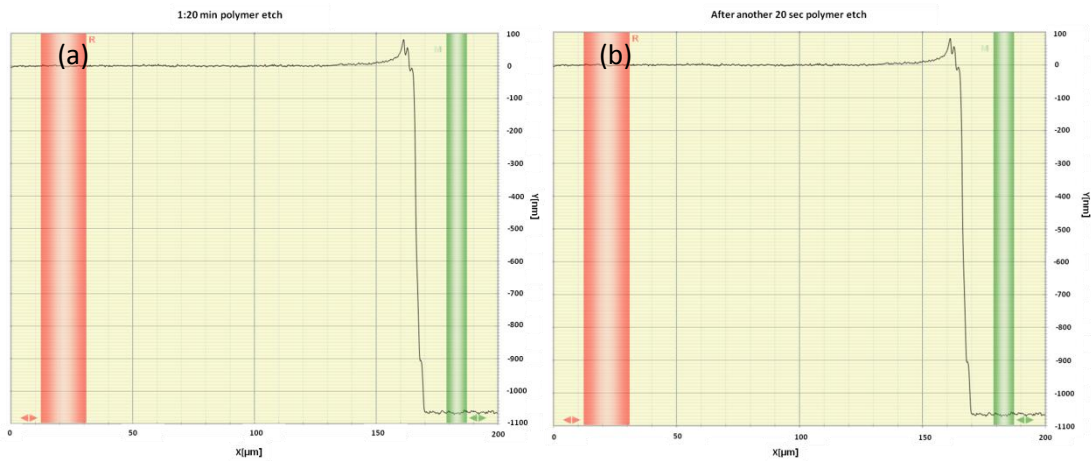


**Figure 4.25:** a. 1:20 sec of polymer etch b. after another 20 sec of polymer etch.

We decided to examine a thicker PR layer. Therefore we used 750nm of Mn-N PR as a result of the 1:2 selectivity. The lithography process was the same as mentioned in section 4.4.4 only that the development duration was 2 min rather than 55 sec due to the thicker layer of Mn-N PR. After we applied 80 sec of *polymer etch* we achieved 1680nm trenches (figure 4.26).

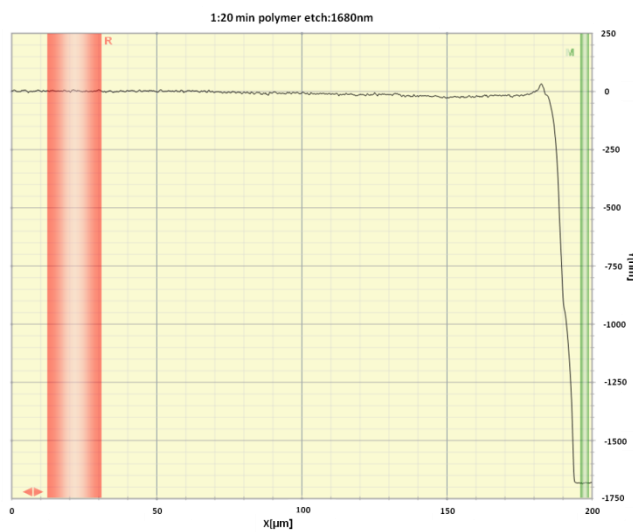


**Figure 4.26:** 1:20 min of *polymer etch*

We concluded that 750nm of PR was sufficient for 1500nm trenches of Cytop. In order to remove the PR remainders we washed the wafer in Acetone and water and dried it in Nitrogen. Further optimization can be done in the width of the PR layer and also in the development duration however removing SiO<sub>2</sub> hard mask layer completely from the structure and using only PR mask was an important contribution for the research.

It is important to mention that due to adhesion problem between Cytop and PFCB the first structure of trench configuration included 3.5µm Cytop, 60nm SiO<sub>2</sub> and another 1.5 µm Cytop (figure 4.27a). This wasn't the ultimate solution since the SiO<sub>2</sub> caused stress to the structure however, the thought was that after the RIE of the structure there will be SiO<sub>2</sub> left at the bottom of the trench which would allow the next PFCB layer to adhere to the Cytop.

We also deposited a 60nm SiO<sub>2</sub> layer in 100°C above the trenches in order to improve adhesion (figure 4.27b) however the same deformations were obtained as in section 4.3.3.2. However, this structure was abandoned after we reached a direct adhesion between Cytop and PFCB as was mentioned in section

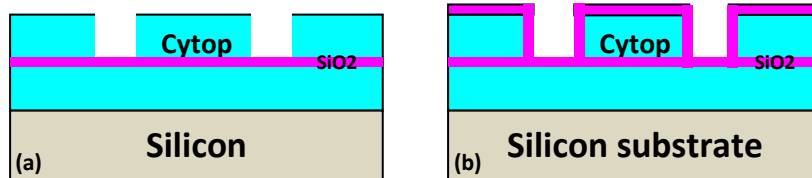
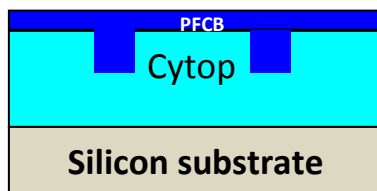


**Figure 4.27:** a. The first structure of "trench" configuration b. Adding SiO<sub>2</sub> adhesive layer

#### 4.4.7 PFCB filling



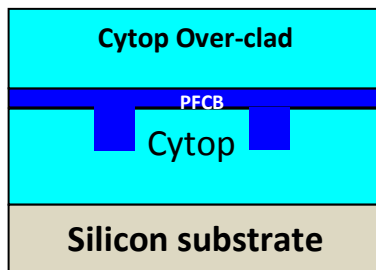
The great challenge in this technique is to fill the trenches with PFCB.

As we mentioned in section 4.3.3.4, we can couple PFCB to Cytop directly by adding Chloroform to the solution and performing plasma ashing before and after spin coating.

However we wished the trenches to be filled completely, which required the PFCB solution to be diluted, achieved by adding more Mesitylene to the solution. We

applied the first step of spin coating (600 rpm for 3 minutes) in order to spread the material homogenously. We then physically spread the PFCB layer using a clean spatula, in order to make sure that the PFCB filled the trenches, and carried on with the second step of the spin coating to determine the thickness beyond the trenches, since we wished to fabricate a ridge waveguide. Therefore the conditions of the second step were: 6000 rpm for 45 seconds in order to get a ridge of 200nm. Finally we inserted the wafer to the oven set to 150°C for 16 hours under an inert environment.

#### 4.4.8 Cytop over-clad



In order to achieve a good adhesion between PFCB and Cytop, it is necessary to apply plasma ashing before spin coating.

The O<sub>2</sub> plasma conditions: 40% power, 0.3 mbar for duration of 30 seconds.

We applied spin coating of Cytop in the following conditions: 600 rpm for duration of 10 minutes followed by 1000 rpm for 45 minutes in order to get 3500nm layer thickness. Finally we inserted the wafer to the oven set to 150°C for 7 hours.

#### 4.4.9 Dicing and polishing

The same as we did in the ridges configuration in section 4.3.10.

Figure 4.28 present an edge facet of the polished square WG.

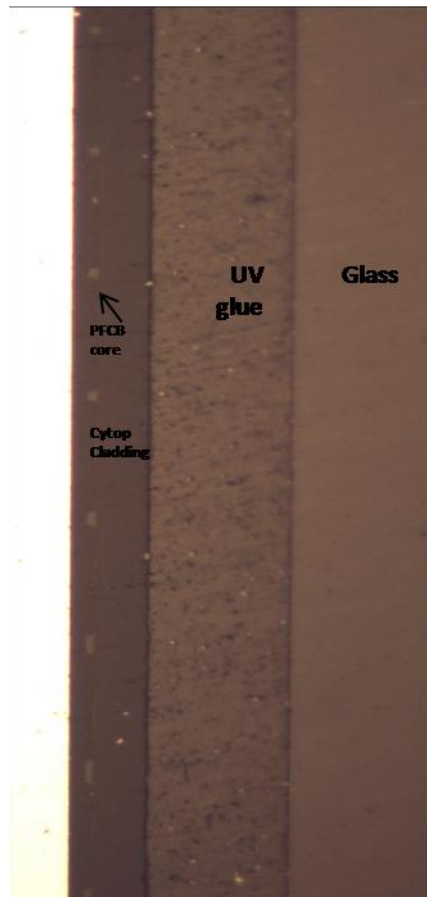
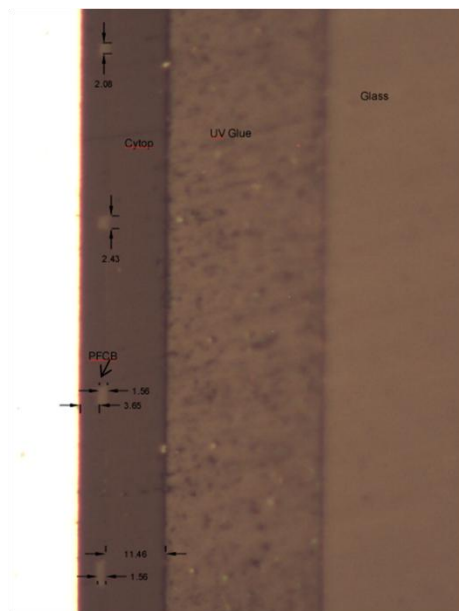


**Figure 4.28:** a cross section of the polished square WG fabricated in the trench method.

## **5 Summary and conclusions**

The purpose of this research was to design a reproducible, NCs compatible fabrication process of a polymeric waveguide made of PFCB core and Cytop cladding. The great challenges in the research were synthesizing the PFCB core material and coupling between PFCB and Cytop layers.

The big contributions of this research were the improvement in the degree of polymerization of the PFCB core polymer. This was achieved by working with 1:9 (TVE:BPVE) monomers ratio rather than 1:1 and also increasing the polymerization temperature to 150°C. Another contribution was the ability to couple directly PFCB and Cytop without using a foreign material to the structure. This was done by performing plasma ashing before and after spin coating and also by adding Chloroform to the PFCB solution. This contribution is significant for reducing the stress and cracks due to CTE mismatch of the materials.

Two configurations of fabrication were examined. The first configuration, ridge WG, dealt with etching the PFCB layer and afterwards burying it with Cytop cladding. In this configuration the additional contribution along with the two mentioned above was using SiO<sub>2</sub> hard mask layer directly on the PFCB layer without forming stress which made the process more controllable rather than placing the SiO<sub>2</sub> hard mask layer above the Cytop over-clad layer. This was achieved due to the ability to synthesize 90% polymerized PFCB which was more rigid and the more compressive and thinner SiO<sub>2</sub> layer.

However this configuration was not completely compatible with the NCs to be embedded in the PFCB core layer since some of the SC NCs materials are not allowed in the RIE machine due to contamination threat. Therefore the second configuration, trench waveguide, was examined.

The big advantage of this configuration over the ridges one is that the only material that went through RIE was the Cytop layer. Therefore we are not limited in the materials which the NCs are made of. We presented several techniques in order to achieve 1500nm trenches in the Cytop layer.

The contribution in this configuration was the ability to achieve the desired trenches without using SiO<sub>2</sub> hard mask. This was done by using Ma-N negative PR which had 1:2 selectivity (PR: Cytop) . This contribution was very significant both in term of stress and in term of fabrication simplification.

Future work will deal with doping the PFCB core with SC NCs. Both ridge and trench configurations will be used. The ridge method will be used with SC NCs materials that are allowed into the RIE chamber. These materials have high third order susceptibility but not high permanent dipole moment constant which means that we will not be able to align them. RIE of *polymer etch* will be applied and sidewalls roughness will be observed. The channel method will be used with SC NCs with both high third order susceptibility and high permanent dipole moment constant. The last will allow us to align them in the polarization direction of the optical mode and by that enhance the nonlinear response. The alignment will be done by adding electrodes within the structure in order to apply an aligning electric voltage on the PFCB and NCs composite during curing in the oven. The electrodes will be as close as possible to the core (minimum of  $3.5\mu\text{m}$  to avoid leakage of the optical mode to the electrodes). Finally we wish to characterize the linear and nonlinear behavior in term of propagation loss, bend loss and nonlinear coefficient.

## References

- [1] A. Adler, Dan M. Marom, High Index Contrast Polymer Optical Waveguides, M.Sc. Thesis (2011).
- [2] P. Agrawal, Nonlinear Fiber Optics, Third addition, Rochester, New York: Academic Press (2001).
- [3] Y. K. Olsson, G. Chen, R. Rapaport, D. T. Fuchs, V. C. Sundar, J. S. Steckel, M. G. Bawendi, A. Aharoni, U. Banin, "Fabrication and optical properties of polymeric waveguides containing nanocrystalline quantum dots," *Appl. Phys. Lett.* 85, pp. 4469-4471 (2004).
- [4] Y. Okamoto H. Teng "Synthesis and properties of amorphous perfluorinated polymers", *Chemistry Today* , vol 27 n 4 / July-August (2009).
- [5] K. Okamoto, *Fundamental of Optical Waveguides*. San Diego: Academic Press (2000).
- [6] S. Coe, W. K. Woo, M. G. Bawendi, and V. Bulovi, "Electroluminescence from single monolayers of nanocrystals in molecular organic devices", *Nature (London)* 420, 800 (2002).
- [7] V. I. Klimov, A. A. Mikhailovsky, S. Xu, A. Malco, J. A. Hollingsworth, C. A. Leatherdale, H.-J. Eisler, and M. G. Bawendi, "Optical Gain and Stimulated Emission in Nanocrystal Quantum Dots," *Science* 290, 314-317 (2000).
- [8] C. B. Murray, C. R. Kagan and M. G. Bawendi, "Synthesis and characterization of monodisperse nanocrystals and close-packed nanocrystal assemblies", *Annual Review of Materials Science*, *Annu. Rev. Mater. Sci.* (2000) **30**, Pages: 545-610
- [9] M. T. Harrison, S. V. Kershaw, M. G. Burt, A. L. Rogach, A. Kornowski, A. Eychmüller, and H. Weller, "Colloidal nanocrystals for telecommunications. Complete coverage of the low-loss fiber windows by mercury telluride quantum dots", *Pure Appl. Chem.*, Vol. 72, pp. 295–307, 2000.
- [10] Liang-shi Li and A. Paul Alivisatos, "Origin and Scaling of the Permanent Dipole Moment in CdSe Nanorods", *Phys. Rev. Lett.* 90, 097402 (2003).
- [11] M. T. Harrison, S. V. Kershaw, M. G. Burt, A. L. Rogach, A. Kornowski, A. Eychmüller, and H. Weller, "Colloidal nanocrystals for telecommunications.

- Complete coverage of the low-loss fiber windows by mercury telluride quantum dots", *Pure Appl. Chem.*, Vol. 72, pp. 295–307, 2000.
- Vol. 72, Nos. 1–2, pp. 295–307 (2000).
- [12] O. Millo, D. Steiner, D. Katz, A. Aharoni, S. Kan, T. Mokari, and U. Banin, "Transition from zero-dimensional to one-dimensional behavior in InAs and CdSe nanorods," *Physica E* 26, pp. 1-8 (2005).
- [13] J. C. Maxwell-Garnett, "Colours in Metal Glasses and in Metallic Films", *Philos. Trans. R. Soc. London, Ser. A* 203, 385-420 (1904).
- [14] R. J. Gehr and R. W. Boyd, "Optical Properties of Nanostructured Optical Materials", *Chemistry of Materials*, (1996).
- [15] A. Shinji, M. Tohru , and S. Shigekuni , " Per fluorinated Polyimide Synthesis", *Macromolecules* (1992).
- [16] J. Ballato and S. Foulger, "Optical properties of perfluorocyclobutyl polymers", *J. Opt. Soc. Am.B*, Vol. 20, No. 9, (2003).
- [17] J. Ballato, S. H. Foulger, D. W. Smith, "The Optical Properties of Perfluorocyclobutyl Polymers II: Theoretical and Experimental Performance," *Josa B*, vol. 21, Issue 5, pp. 958-967 (2004).
- [18] J. Gordon, J. Ballato, D. W. Smith "optical properties of perfluorocyclobutyl polymers. III. Spectroscopic characterization of rare-earth-doped perfluorocyclobutyl polymers", *J. Opt. Soc. Am.B*, Vol. 22 ,Issue 8, pp. 1654-1659 (2005).
- [19] Dennis w. Smith,Jr., Shengrong Chen, Suresh M. Kumar, John Ballato, Chriss Topping, Hiren V. Shah, and Stephen H. Foulger, "perfluorocyclobutyl copolymers for microphotronics" *Advance Materials*. 14,No. 21,November 4 (2002).
- [20] H.R. Brown , "Adhesion Between Polymers and Other Substances - A Review of Bonding Mechanisms, Systems and Testing", *Materials Forum*, Vol. 24, pp. 49-58, (2000).
- [21] Attila F. Pavlath "plasma treatment of natural materials" (1974).
- [22] E. Plueddemann, "Silane Coupling Agents" (1982).
- [23] O. Ziemann, J. Krauser, P. E. Zamzow, W.Daum, *POF Handbook, Optical Short Range Transmission Systems* (2008).

- [24] C. Koos, L. Jacome, C. Poulton, J. Leuthold and W. Freude, "Nonlinear silicon-on-insulator waveguides for all-optical signal processing", *Opt. Express* 15, 5976–5990 (2007).
- [25] Y. Lior, Dan M. Marom, Nonlinear Optical Waveguides from Dilute Composites Consisting of Polymer with Partially Aligned Nanorods, M.Sc. Thesis (2012).
- [26] F. Ladouceur and J. D. Love, *Silica-based Buried Channel Wave-guides and Devices*. Chapman & Hill (1996).
- [27] A. Yenyay and R. Gao, "nanoporosity effect in optical loss of single-mode polymer waveguide" *Applied Optics*, Vol. 49, Issue 19, pp. 3684-3690 (2010).
- [28] N.Sugiyama, in: J. Scheirs (Ed.), "Modern fluoropolymers", Wiley ,p. 541 (1997).
- [29] N. Rahmanian, "high efficiency perfluorocyclobutyl air-trench splitters for use incompact ring resonator", Alabama (2007).